

We thank the reviewers for their time and comments, which are reproduced in *italic font* below. Our responses are shown in regular font. Text added to the manuscript is underlined.

*Anonymous referee #1*

*General comment: This paper presented a newly developed IBBCEAS system for measuring ambient HONO and NO<sub>2</sub>. The subject is within the scope of the journal, but the IBBCEAS techniques is not a new technique for measuring HONO and NO<sub>2</sub>. There are several papers with the same topic had been published in AMT recently (like Min et al., 2016; Duan et al., 2018). The authors should make it clear that what is new in this work.*

Response: We appreciate the reviewer's point of view. The novelty of this paper is threefold:

- (a) We describe a newly constructed instrument that has not been previously described,
- (b) we validate the HONO response of the IBBCEAS via a comparison to blue diode laser TD-CRDS, which as far as we know has not been previously made, and
- (c) we show sample ambient air data that have not been previously published.

Since novelty is a given (i.e., can be taken for granted) in any scientific manuscript and in our opinion the novelty of this work is transparent, we have chosen not to amend the manuscript in response to this comment.

*The authors also should be more conservative, especially when using the statement like "state-of-the-art". Compared with the previous instruments mentioned before, this instrument (HODOR) does not have the best detection capacity in fact. The following comments should be addressed.*

Response: Our apologies - we used the phrase "state-of-the-art" with a common dictionary definition of "the most recent stage in the development of a product, incorporating the newest ideas and the most up-to-date features" but realize that it could also be interpreted as "the most recent and therefore considered the best; up-to-the-minute". In response to the reviewer's comment, we have removed the adjective "state-of-the-art" from the abstract and added the underlined words to the sentence on line 355 as follows:

"The 60 s HODOR LOD was 240 pptv and of similar magnitude as the LODs of 180 pptv reported by Duan et al. (2018) and of 200 pppv Nakashima and Sadanaga (2017) and hence on par with state-of-the-art instruments."

*Specific comments:*

*1. The fitting results showed in Fig. 4 have some problem, especially the fitting range from 365 to 370 nm. It seems that the measured HONO absorption coefficient (orange line) is quite similar to the unconvoluted cross section from Stutz et al., 2000 (may be the convolution is not so good). The author should give some explanations of the large residual.*

Response: We agree with the reviewer that the residual ought to be void of structure. As stated in the text (lines 158-163), we convoluted the reference spectra using the observed width of a Ne line

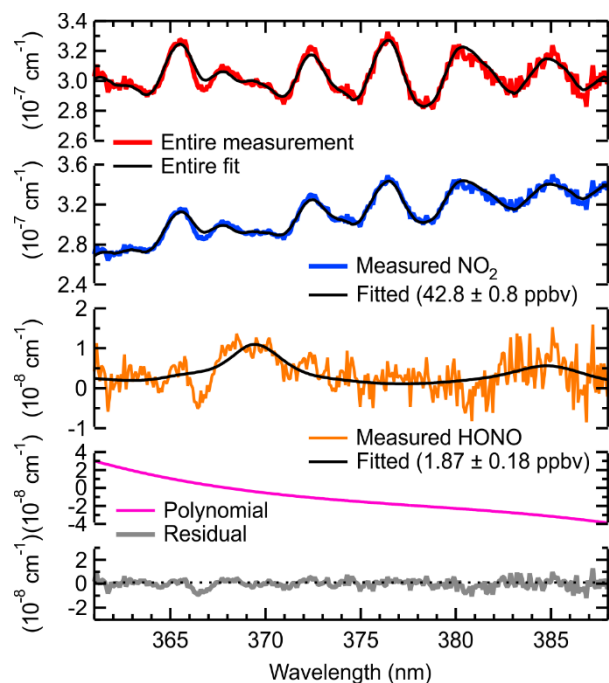
(1.04 nm). It certainly appears that the convolution between 365 and 370 nm may have been too aggressive, perhaps. The largest feature in the residual spectrum lines up with a trough in the NO<sub>2</sub> spectrum, whereas the second largest feature in the residual spectrum is located at the HONO peak (but is narrower). Outside this wavelength region, the agreement between observed and fitted spectra seems better. We cannot offer an explanation as to why that occurs but agree with the reviewer that a likely culprit is the instrument function used.

We acknowledged this issue in the conclusion section (see statement on lines 370-375 reproduced below). During the review phase, we were also made aware of a paper by Kleffman et al. (2006) who noted that some literature NO<sub>2</sub> absorption cross-sections contain HONO as an impurity.

"One of the challenges we encountered in the accurate retrieval of NO<sub>2</sub> and HONO was the convolution procedure and choice of cross-section. Literature values for NO<sub>2</sub> vary by up to  $\pm 6.2\%$  (Harder et al., 1997; Burrows et al., 1998; Vandaele et al., 1998), such that the choice may introduce a systematic bias. In addition, some NO<sub>2</sub> reference spectra have been reported to contain HONO as an impurity (Kleffman et al., 2006). Though not performed in this work, it may be advisable to use one's own reference spectra in future IBBCEAS NO<sub>2</sub> and HONO retrievals."

*I also suggest the authors show the spectral fitting results from ambient measurement or the lab result of relatively low NO<sub>2</sub> and HONO, which would be more representative.*

Response: We have prepared such a figure as requested (see below). This particular spectrum was acquired on April 27, 2018, at 1:00 MST. Mixing ratios of  $42.8 \pm 0.8$  ppbv of NO<sub>2</sub> and  $1.87 \pm 0.18$  ppbv of HONO were retrieved.



We have updated the text in section 3.4:

Original: "Figure 4 shows an example fit containing NO<sub>2</sub> and HONO from a sample generated using the HONO generation system described in Sec. 2.6. The top panel shows the entire absorption (and the fit shown in black) along with the scattering coefficient of air. In this example, NO<sub>2</sub> (shown in blue) and HONO (shown in orange) mixing ratios of 109±0.2 ppbv and 23.9±0.4 ppbv were obtained, respectively."

Revised: "Figure 4 shows an example fit containing NO<sub>2</sub> and HONO in ambient air, collected on April 27, 2018, at 01:00 MST. The top panel shows the entire absorption (and the fit shown in black) along with the scattering coefficient of air. In this example, NO<sub>2</sub> (shown in blue) and HONO (shown in orange) mixing ratios of 42.8±0.2 ppbv and 1.9±0.2 ppbv were obtained, respectively."

We also updated the caption of Figure 4.

Original: "**Figure 4** Sample fit for laboratory generated NO<sub>2</sub> and HONO samples at 879.9 hPa and 296 K. The top panel shows the entire absorption spectrum. Shown below are the absorption spectra of NO<sub>2</sub> and HONO with their respective fit errors and the polynomial. The bottom panel shows the fit residual."

Revised: "**Figure 4** Sample fit of ambient air containing NO<sub>2</sub> and HONO sampled on April 27, 2018, at 01:00 MST. The top panel shows the entire absorption spectrum. Shown below are the absorption spectra of NO<sub>2</sub> and HONO with their respective fit errors and the polynomial. The bottom panel shows the fit residual."

*2. The insert plot of Fig. 5b showed that the zero only had one point in each cycle. The author should check the transient time of mode changing from sampling mode to zero mode to make sure the zero mode without HONO.*

Response: Data were acquired at 10 s, and fit results of the 10 s data were averaged to 60 s (which is the time resolution shown in the Figure). The transient time was checked. Figure S7 in the supplemental material section shows this at 1 s time resolution.

No changes were made to the manuscript.

*3. Figure 5. The blue region represents lab sample and grey region represents zero, so what is the white region mean (Line 284, text indicated the indoor ambient air)?*

The regions that are not color-coded (and hence appear white) are a combination of synthetic air or lab air to which various amounts of synthetic air containing HONO, NO<sub>2</sub> and zero air were added. We have modified the figure caption as follows:

**Original:** "**Figure 5** Time series of NO<sub>2</sub> and HONO mixing ratios for synthetic and laboratory air, averaged to 1 min. **a)** ...."

**Revised:** "**Figure 5** Time series of NO<sub>2</sub> and HONO mixing ratios observed by HODOR, CRDS and TD-CRDS, averaged to 1 min. The instruments sampled for zero air (grey underlay), laboratory air (blue underlay) and laboratory air to which varying amounts of synthetic air containing NO<sub>2</sub>, HONO and zero air were added (white underlay). **a)** ...."

*Why TD-CRDS only has such short measurement time period?*

Response: The TD-CRDS HONO measurement is only valid when HONO is fully dissociated to NO (which is then oxidized in excess O<sub>3</sub> to NO<sub>2</sub>). For the time period 23:30 - 00:10 of Figure 5, the TD-CRDS inlet converter temperature was ramped up and down several times to acquire thermograms (i.e., plots of signal vs. inlet temperature; an example is shown in Figure S4). The handful of data points shown in Figure 5b were collected when inlet temperatures were > 520 °C. After 00:10 of Figure 5, the TD-CRDS inlet temperature was constant (average ± 1 standard deviation of 523 ± 3 °C).

When sampling laboratory air the TD-CRDS does not have the necessary sensitivity to detect let alone quantify HONO since there is a large NO<sub>x</sub> background that needs to be subtracted, as stated on line 287:

"In contrast to the IBBCEAS instrument, the TD-CRDS instrument was unable to quantify HONO in indoor air since the high NO<sub>2</sub> background introduces a large subtraction error in the heated channel."

In response to the reviewer's comment, we added the following to the caption of Figure 5:

**"b) HONO mixing ratios reported by TD-CRDS (black) and IBBCEAS (orange). From 23:30 to 00:10, the TD-CRDS inlet converter temperature was ramped up and down several times to collect thermogram; only data collected at an inlet temperature >520 °C are shown here."**

*As the authors mentioned that GNOM suffered with interference of high NO2. I do not think the inter-comparison of HODOR with GNOM is appropriate to prove the measurement capacity of HODOR in measuring HONO.*

Response: We, respectfully, disagree with the reviewer as TD-CRDS is quite accurate indeed when sampling a dilute mixture of HONO in zero air, i.e., in the absence of a large NO<sub>x</sub> background. This is exemplified by the high degree of correlation as stated on lines 290-:

"The scatter plot of IBBCEAS vs. TD-CRDS HONO data (Fig. S6b; only data points when the synthetic source was sampled were included in the fit) has a slope of 1.01±0.01, an intercept of 0.01±0.24 ppbv and r<sup>2</sup> of 0.995. "

No changes were made to the manuscript in response to this comment.

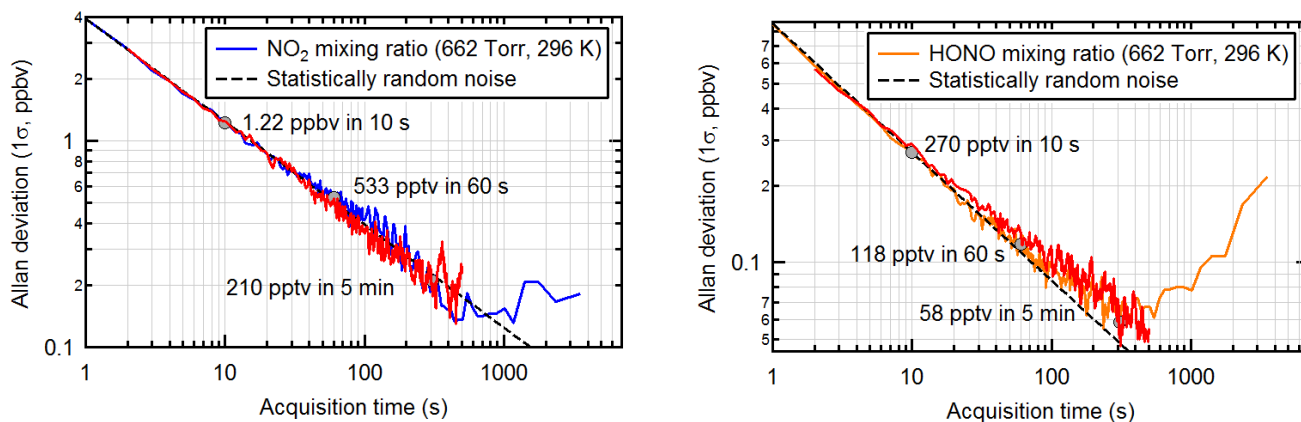
*4. Allen deviation only used to study the system stability, the instrumental limit of detection should be characterized by the standard deviation. Figure 6 showed that the zero measurement results (here time resolution is 1 s?), and the LOD can be derived from the data. According to the result from Figure 6, the LOD for measuring HONO may be several hundred ppt (1 sigma).*

Response: The reviewer is correct that Allan variance may (or may not) equal the usual variance, from which detection limits are calculated. Werle et al. (1993) state that "in the case of a white-noise dominated system, the Allan variance is equivalent to the variance of the mean and, as the variance of the mean is a measure for the detection limit, the Allan variance can be used to predict the detection limit." We added the following on line 298:

"Allan deviation analyses (Werle et al., 1993) ..... This analysis also allows an estimate of the LOD for each molecule for white-noise dominated data (Werle et al., 1993)."

In light of the reviewer's comment, we calculated standard deviations of the data shown in Figure 6 when averaged over 2, 3, 4, etc. seconds. We added those standard deviations to the plots in Figure 6 (in red color) and included those plots in our response here.

For NO<sub>2</sub>, the Allan and standard deviations give quasi-equivalent results. For HONO, the results were dependent on the length of the data sample averaged: When all data were included, the plot resembled Fig. 6 of (Duan et al., 2018) because the average (used in the calculation of standard deviation) is "moving" i.e., changes due to drift. When a shorter segment (~2,000 seconds) of data are averaged, the Allan and standard deviations are also quasi-equivalent (see graph below). Hence, the use of Allan deviation to estimate the LOD is justified.



5. Line 110. How about the temperature control of CCD in the operation?

Response: The CCD was Peltier-cooled to -80 °C when in operation. We added the following on line 132:

"The instrument was turned on 30 min prior to measurements to allow for the LED temperature to stabilize and the CCD camera to cool to its operating temperature of -80 °C."

Minor comments:

6. Line 160. Temperature sensor and pressure sensor mentioned are missed in Fig. 1.

Response: We modified the text section as follows:

".. the temperature and pressure of the sampled gas, monitored using a K-type thermocouple (Omega) attached to the sample cell holder and a pressure transducer (MKS Baratron 722B) located next to where gases exit the sample cell and upstream of the mass flow controller."

7. Line 103. Please add the manufacturer information of the spectrometer.

Response: We inserted the requested information: "The grating spectrometer (spectrograph and camera; Princeton Instruments Acton SP2156) has been described by Jordan et al. (2019)."

8. Line 125-130. The purity of N<sub>2</sub> and Ar should be given.

Response: The gas purities are stated in Table 2. No changes were made in response to this comment.

9. Is the "celllength" the same as "cavity length" in the text, please unify.

Response: Corrected as requested.

10. Unify the font size of the title of Section 3.4

Response: Corrected as requested.

11. Line 356. pppv correct to pptv

Response: Fixed. Thank you.

*Anonymous referee #2*

*The manuscript describes a new instrument for the detection of HONO using cavity enhanced absorption spectroscopy. The paper is well written and gives a detailed description of the detection method. It is well suited for the journal. I recommend publication after addressing the following points:*

*I am missing a more detailed discussion of potential interferences from for example HONO formation / conversion of nitrogen oxide species in the inlet system. Did the authors do any kind of tests to exclude that HONO is artificially formed in the inlet system?*

Response: We agree with the reviewer that inlet artefacts are an important consideration for any instrument when sampling ambient air. In our instrument, all wetted surfaces in the inlet system were constructed from inert FEP Teflon tubing and PFA fittings. We observed fast rise times when adding HONO to the inlet and equally fast fall times when zeroing (e.g., Figure S7) and hence do not believe that partitioning of HONO to or from the inner walls of the inlet was significant in the experiments presented here. We also did not notice any evidence for formation of HONO within the inlet system. Having said this, we agree that if the instrument is deployed for longer-term ambient air measurement, the inlet system needs to be scrutinized more. The following was added on line 336 (in the section on accuracy):

"Not included in this estimate are potential systematic errors resulting from the spectral convolution and fitting procedure (Sect 2.4), ~~and~~ photolysis of the fitted species within the optical cavity, and potential inlet artefacts (which were not characterized under atmospheric conditions)."

The following was added to the conclusion on line 382:

"Though not examined in this work, interferences may arise when sampling for long periods in heavily polluted environments from soot deposition on inlet filters and walls. In such situations, it would be advisable to monitor inlets for HONO production (or loss) upon aging, for example using a setup as recently described by Duan et al. (2018)."

*The potential of such interferences are also not mentioned in the introduction (page 2 line 36).*

Response: We agree that this should have been mentioned and have added the following on line 43:

"A considerable advantage of open-path instruments is the lack of any inlet and associated chemistry, such as loss of HONO due to partitioning onto inlet walls (Duan et al., 2018) or HONO formation, for example from reaction of NO<sub>2</sub> with soot particles (Longfellow et al., 1999; Kalberer et al., 1999; Indarto, 2012) that may have deposited on the inlet lines and particle filter."

*It should be mentioned that interferences are detected and corrected for in LOPAP instruments (page 2 line 33-35).*

Response: We have added the following statement: "In practice, interference from NO<sub>2</sub> and O<sub>3</sub> can be accounted for with a two-channel system and interference from PAN can be avoided by sampling at low pH (Kleffmann et al., 2006). Interference from HO<sub>2</sub>NO<sub>2</sub> is likely only significant in cold environments such as the poles since this compound is prone to thermal decomposition (Legrand et al., 2014)."

*What was the purity of the NO used for the production of NO<sub>2</sub> by ozone titration? Was there any artificial signal observed from impurities in the NO cylinder (page 7, line 180)?*

Response: Apologies for omitting this. The cylinder was supplied by Scott-Marrin and was filled with (101±1) ppmv nitric oxide in oxygen-free and moisture-free nitrogen. Scott-Marrin certified an NO<sub>2</sub> content of <0.5 ppmv. In practice, the amount of NO<sub>2</sub> emitted was larger (mainly because the oxygen-free nitrogen was combined with pure oxygen prior to delivery (Figure 1C) - if nitrogen was used as a ballast, the NO<sub>2</sub> content was negligible). On occasion, we monitored the NO<sub>2</sub> and NO<sub>x</sub> output of the gas delivery system in two parallel CRDS channels and typically found a ratio of 1.85% NO<sub>2</sub> in NO<sub>x</sub>.

Another important detail that we should have mentioned that once the setup used to deliver NO<sub>2</sub> was assembled, it always remained under flow of oxygen to keep moisture and impurities that might be present in room air (e.g., HNO<sub>3</sub> or HONO) out of the lines, i.e., to keep the tubing dry and clean.

We added the following on line 184:

"Briefly, NO<sub>2</sub> was generated by mixing the output of a standard NO cylinder (Scott-Marrin, 101±1 ppmv in oxygen- and moisture-free nitrogen)" with O<sub>3</sub> produced by illuminating a flow of O<sub>2</sub> (99.99%, Praxair) by a 254 nm Hg lamp followed by dilution with zero air to vary the product concentration. When not in

use, the setup remained under O<sub>2</sub> flow to prevent moisture and other impurities from contaminating the tubing."

*What is the precision and accuracy of the conversion efficiency (the number of digits given here suggests a very high precision) (page 8 line 217)?*

Response: We agree with the reviewer that the number of digits used is optimistic. The value 83.8% was derived from a box model simulation which is precise as far as the computation is concerned, but of course relies on several assumptions, such as rapid mixing of the added ozone with the sample gas and accuracy of rate coefficients. The most important uncertainty is the rate coefficient for NO + O<sub>3</sub>, which NASA/JPL puts at ±10%.

We added the following on line 227: "The accuracy of this correction factor is limited by knowledge of the rate coefficient for the oxidation of NO by O<sub>3</sub>, ±10% (Burkholder et al., 2015)."

*Are the measurements in Fig. S4 examples for a typical measurement or can the measurements repeated with high accuracy that always the same concentrations are observed (page 8 line 221-225)?*

Response: This is an example of a typical measurement. With the HONO source used in this work, it was challenging to always produce the same concentration; however, this didn't matter in practice since scatter plots of the two measurements were ultimately generated (e.g., Figure S6b). We have modified the section of text as follows:

"Figure S4 shows a sample TD-CRDS inlet temperature scan when the output of the source described in Sec. 2.6 was sampled. In this particular example, the heated channel (to which excess O<sub>3</sub> was continuously added) measured ~137.5 ppbv of NO<sub>y</sub> (NO<sub>x</sub> + HONO) ..."

*Did the authors have a closer look, if the intercept in the regression for lab measurements holds for low NO<sub>2</sub> values (page 10 line 290)? For ambient air measurements, this would be a significant source of errors, but might be here due to the large range of values here.*

Response: We agree with the reviewer that intercept is larger than desired and is driven by the large range of values as the reviewer states. No changes were made.

*Was the GNOM instrument running in parallel also during ambient air measurements (section 3.8)? If so could the authors show the correlation of NO<sub>2</sub> with the HODOR instrument? I would prefer to see the regression analysis in the main paper.*

Response: Unfortunately, the GNOM instrument was not operated during the ambient air measurements. No changes were made.



*Anonymous referee #3*

*General comments: This is a really well written manuscript on the development of an IBBCEAS instrument at the University of Calgary, operated in the near UV between 361 and 388 nm for the detection of HONO and NO<sub>2</sub>. Even though the authors pay excellent attention to experimental detail and characterize the performance comprehensively, including first measurements in ambient air, the technology in this manuscript, the measurement principles, the calibration approaches and verification methods are all known and not really new. Despite the very competent experimental description of the instrument, in my opinion, the manuscript is lacking novelty as illustrated in Table 1, where 7 other publications are listed using the same or very similar broadband cavity enhanced approaches. The authors themselves recently published a very similar instrument merely in a different spectral region. The most novel aspect in this manuscript concerning the area of 'CEAS for field detection of trace gas species' lies in the comparison of IBBCEAS with TD-CRDS, which is very brief in terms of a discussion and largely kept in the supplementary material. If the work is deemed publishable by the editorial board, then material from the supplementary material (S6,S7) should be moved into the main body of the text and further discussed.*

Response: We thank the reviewer for this frank assessment. Briefly, the novelty of this paper is  
(a) We describe a newly constructed instrument that has not been previously described,  
(b) we validate the HONO response of the IBBCEAS via a comparison to blue diode laser TD-CRDS, which as far as we know has not been previously made, and  
(c) we show sample ambient air data that have not been previously published.

Regarding the suggestion by the reviewer to reorganize the manuscript. The focus of this manuscript is on the new IBBCEAS, not on TD-CRDS, and we prefer to keep the manuscript focused on the CEAS. The supplemental material is posted on the publisher's web site in any case and is discerned to the community, so there is no need to reorganize the manuscript.

No changes were made in response to this comment.

*The work would gain substantial merit from an investigation of the performance of the instrument in field applications especially under various experimental conditions and atmospheric environments. The long-term performance of IBBCEAS instruments in the field under more or less harsh conditions has not been scrutinized to a high standard in the literature yet, but this was unfortunately not within the scope of this work.*

Response: We agree with the reviewer that a thorough assessment of the in-field performance of this instrument (and the inlet in particular) will be the next step. The following was added to the conclusion section:

"Though not examined in this work, interferences may arise when sampling for long periods in heavily polluted environments from soot deposition on inlet filters and walls. In such situations, it would be advisable to monitor inlets for HONO production (or loss) upon aging, for example using a setup as recently described by Duan et al. (2018)."

*A few observations and comments in detail:*

*- The light source has an emitting area of 1.4x1.4 mm<sup>2</sup> ... (I79)*

Response: The text was modified as suggested.

- 1200 grooves  $\text{mm}^{-1}$ ... (I104)

Response: We thank the reviewer for catching this typo. It has been fixed.

- (Kraus, 2003) is missing in the reference list (I156).

Response: Our apologies. For some reason, the reference management software keeps removing this citation from the bibliography. It is Kraus, S.: DOAS Intelligent System Version 3.2.3505, Institute of Environmental Physics, University of Heidelberg, available at: <https://doasis.iup.uni-heidelberg.de/bugtracker/projects/doasis/> (last access: 31 August 2018), 2003. and has been added to the reference list.

*More information on the DOASIS retrieval could be given here.*

Response: More information (such as range fitted, allowed spectral shifting, order of polynomial used in the fit, etc.) was given further down in the paragraph. We moved the sentence "Gas concentrations were extracted from a linear least square fit applied to the calculated absorption coefficient, followed by conversion to mixing ratios using the number density of air calculated from the ideal gas law and the temperature and pressure of the sampled gas, monitored using a K-type thermocouple (Omega) attached to the sample cell holder and a pressure transducer (MKS Baratron 722B) located next to where gases exit the sample cell and upstream of the mass flow controller." to the end of the paragraph to make this clearer.

- third-order ... (I162)

Response: The text was modified as suggested.

- *The inlet was guided through a partially open window. How far from the outside surface of the wall or window was the inlet line? How long was it? Was the instrument facing N,W,S, or E?*

Response: The instrument sampled from a 1.8 m long FEP Teflon inlet at a flow rate of 2 slpm, with approximately 1/3 of the inlet line (~2 feet) protruding from the window. The window and inlet faced SE. We modified a sentence on line 247 from "The instrument's inlet was guided through a partially open window." to "The instrument sampled from a 1.8 m long FEP Teflon™ inlet at a flow rate of 2 slpm, of which ~1/3 was guided through a partially open window."

*What can the authors say about losses in the inlet line. (p8 bottom and also p12)*

Response Reviewer #2 also inquired about this issue. In short, Inlet artefacts are an important consideration for any instrument when sampling ambient air. In our instrument, all wetted surfaces in

the inlet system were constructed from inert FEP Teflon tubing and PFA fittings, plus we observed fast rise times when adding HONO to the inlet and equally fast fall times when zeroing (e.g., Figure S7). We hence do not believe that partitioning of HONO to or from the inner walls of the inlet was significant in the experiments presented here. We also did not notice any evidence for formation of HONO within the inlet system. Having said this, we agree that if the instrument is deployed for longer-term ambient air measurement, the inlet system needs to be scrutinized more. The following was added to the introduction on line 43:

"A considerable advantage of open-path instruments is the lack of any inlet and associated chemistry, such as loss of HONO due to partitioning onto inlet walls (Duan et al., 2018) or HONO formation, for example from reaction of NO<sub>2</sub> with soot particles (Longfellow et al., 1999; Kalberer et al., 1999; Indarto, 2012) that may have deposited on the inlet lines and particle filter."

The following was added on line 336 (in the section on accuracy):

"Not included in this estimate are potential systematic errors resulting from the spectral convolution and fitting procedure (Sect 2.4), and photolysis of the fitted species within the optical cavity, and potential inlet artefacts (which were not characterized under atmospheric conditions)."

The following was added to the conclusion on line 382:

"Though not examined in this work, interferences may arise when sampling for long periods in heavily polluted environments from soot deposition on inlet filters and walls. In such situations, it would be advisable to monitor inlets for HONO production (or loss) upon aging, for example using a setup as recently described by Duan et al. (2018)."

*- In addition to the opening paragraph, there is also merit in the Rayleigh scattering cross-section measurements, as they confirm measurements in the literature from some time ago.*

Response: We agree.

No changes were made.

*- Cleanliness: : : (I268)*

Response: Typo has been corrected. Thanks for catching this.

- *The fact that the background in Fig. 4 is quite substantial and negative is not discussed in the manuscript. (p10)*

Response: Fig. 4 has been replaced. Please also see our response to reviewer #1.

- *The authors explain that the common approach in the literature to determine the LOD is not following the more strict recommendation of IUPAC, however, then they do not follow the recommendation either, as far as I can see. (p11)*

Response: This is correct. The argument by Loock and Wentzell is based on the notion that the detection limit should be determined by determining the standard deviation of repeated measurements of at least one concentration near the LOD, rather than via repeated measurements of a blank as it is commonly done. The experimental challenge, of course, is to make sure that a stable, low concentration is indeed delivered.

No changes were made.

- *The authors list a set of errors limiting the accuracy of their measurements and classify them as random. The literature cross-sections for the retrieval is a systematic error. The mirror reflectivity and RL are also systematic for a given set of measurements, until they are measured again. (p11)*

Response: This is correct. What we had meant to say that these errors are independent from each other. We have removed the phrase "and random" and clarified that we added these uncertainties in quadrature (following how errors were propagated by (Min et al., 2016)).

- *higher flow rate... (I330)*

Response: The text was modified as suggested.

- *pptv (typo I356)*

Response: Fixed.

- *The LED does not seem to emit between 330 and 400 nm as stated in the caption (I558)*

Response: Indeed, the cavity output below ~350 nm is negligible. The superficial phrase "broadband (330 - 400 nm)" was removed.

- *The effective pathlength... (I560)*

Response: The text was modified as suggested.

- In Figure 5 the "blue time" and "grey time" are explained, the "white times" are unclear.

Response: Reviewer #1 also pointed this out - the caption has been changed as follows:

**Original:** "Figure 5 Time series of NO<sub>2</sub> and HONO mixing ratios for synthetic and laboratory air, averaged to 1 min. a) ...."

**Revised:** "Figure 5 Time series of NO<sub>2</sub> and HONO mixing ratios observed by HODOR, CRDS and TD-CRDS, averaged to 1 min. The instruments sampled for zero air (grey underlay), laboratory air (blue underlay) and laboratory air to which varying amounts of synthetic air containing NO<sub>2</sub>, HONO and zero air were added (white underlay). a) ...."

(p23) - Specify the term "+/-1σ measurement uncertainty" in the caption further or include a cross-reference. (I575)

Response: We have removed the "±1σ" from the caption of Figure 5.

- ...sample ambient air data... improve phrase, caption Figure 7 (I586)

Response: The first phrase of the caption of Figure 7 was changed from "Time series of sample ambient air data averaged to 5 min." to "Sample ambient air data."

*Anonymous referee #4*

*This paper shows the new instrument for the simultaneous measurements of ambient HONO and NO<sub>2</sub> by BBCEAS, and its assessment. This paper is well written and the authors pay attention to the analysis. Unfortunately, it is not "novel" technique for the ambient measurements of HONO and NO<sub>2</sub> by BBCEAS because there are many similar reports, as authors show. However, there is a little example for the application of the BBCEAS to the ambient measurements for the trace species. In addition, the comparison of the simultaneous measurements of HONO and NO<sub>2</sub> between IBBCEAS and the other technique is important. Therefore I recommend that this paper is published after the clarification some questions shown below.*

*1. For this instrument, there is no some experimental conditions. What company do you use for the spectrometer and CCD camera?*

Response: We inserted the requested information (on line 103):

"The grating spectrometer (spectrograph and camera; Princeton Instruments Acton SP2156) has been described by Jordan et al. (2019)."

*How much is the flow rate of the sample/ambient air (important information due to the next concern)?*

Response: As stated on line 140, "Air was sampled at a flow rate of 2–3 slpm". No changes were made to the manuscript.

*2. For the intercomparison of the simultaneous measurements of HONO and NO<sub>2</sub> by BBCEAS and TD-CRD, the authors tried to the estimation of the effects of the NO titration and NO<sub>2</sub> oxidation by box model. In this experiments, the concentration of HONO is 23.9 ppbv. Therefore, the OH radicals must be produced the same concentration in the TD cell. I think the concentration of OH radical can not ignore compared with that of NO<sub>2</sub> (109 ppbv).*

Comment: In the heated section, HONO dissociates to NO and OH. The NO is oxidized to NO<sub>2</sub> after the heater using excess O<sub>3</sub>. Thus, in the heated section, most of the NO<sub>x</sub> is present as NO. If OH reacts with NO, it produces HONO, which (thermally) dissociates again.

*In the TD cell, the reaction of OH with NO<sub>2</sub> must be caused and nitric acid must be produced. Womack et al. (Atmos. Meas. Tech., 10, 1911–1926, 2017) shows the temperature and flow rate dependences of the thermal dissociation of nitric acid. According to the Womack's paper, nitric acid may not be dissociate due to the lower temperature under the author's experimental condition. I think that the retrieval of NO<sub>2</sub> may be underestimate due to the formation of nitric acid.*

Response: The conversion temperatures vary between quartz heaters and are a function of residence time. In our experience, the TD profiles of HONO and HNO<sub>3</sub> overlap (and also do for the NOAA instrument - see (Wild et al., 2014)). Also, we observe linear correlations between CEAS and TD-CRDS - two very different measurements - throughout the mixing ranges tested (up to ~100 ppbv). If there were significant secondary effects like HNO<sub>3</sub> formation, we would not expect to see linear correlations with a

parallel measurement. We hence do not agree with the reviewer that HNO<sub>3</sub> formation poses a significant interference.

No changes were made to the manuscript in response to this comment.

*How do the author estimate the effect of the reaction of OH? And do the author consider the effect of the retrieval of HONO on the underestimation of NO<sub>2</sub>?*

Response: It seems that the lifetime of OH within the quartz heaters is rather short since there is no evidence for OH adducts (i.e. HONO or HNO<sub>3</sub> formation). We previously observed similar behaviour with ClNO<sub>2</sub> (Thaler et al., 2011), for which we expected non-linear thermal conversion to NO<sub>2</sub> (due to reaction of Cl with NO<sub>2</sub> to ClNO<sub>2</sub>) but we have never observed that. We can only speculate as to the fate of OH, which may be lost due to collision with the quartz, but may also react with other gas-phase constituents of the sampled air, the bulk of which is generated using a NO<sub>x</sub>-free zero air generation system which may contain light hydrocarbons (e.g., methane).

No changes were made to the manuscript in response to these questions.

## References

- Burkholder, J. B., Sander, S. P., Abbatt, J. P. D., Barker, J. R., Huie, R. E., Kolb, C. E., Kurylo, M. J., Orkin, V. L., Wilmoth, D. M., and Wine, P. H.: Chemical Kinetics and Photochemical Data for Use in Atmospheric Studies, Evaluation Number 18, National Aeronautics and Space Administration, Jet Propulsion Laboratory, California Institute of Technology, Pasadena, California, 2015.
- Burrows, J. P., Dehn, A., Deters, B., Himmelmann, S., Richter, A., Voigt, S., and Orphal, J.: Atmospheric remote-sensing reference data from GOME: Part I. Temperature-dependent absorption cross-sections of NO<sub>2</sub> in the 231-794 nm range, *J. Quant. Spectrosc. Radiat. Transf.*, 60, 1025-1031, 10.1016/S0022-4073(97)00197-0, 1998.
- Duan, J., Qin, M., Ouyang, B., Fang, W., Li, X., Lu, K., Tang, K., Liang, S., Meng, F., Hu, Z., Xie, P., Liu, W., and Häsler, R.: Development of an incoherent broadband cavity-enhanced absorption spectrometer for in situ measurements of HONO and NO<sub>2</sub>, *Atmos. Meas. Tech.*, 11, 4531-4543, 10.5194/amt-11-4531-2018, 2018.
- Harder, J. W., Brault, J. W., Johnston, P. V., and Mount, G. H.: Temperature dependent NO<sub>2</sub> cross sections at high spectral resolution, *J. Geophys. Res.-Atmos.*, 102, 3861-3879, 10.1029/96jd03086, 1997.
- Indarto, A.: Heterogeneous reactions of HONO formation from NO<sub>2</sub> and HNO<sub>3</sub>: a review, *Res. Chem. Intermed.*, 38, 1029-1041, 10.1007/s11164-011-0439-z, 2012.
- Jordan, N., Ye, C. Z., Ghosh, S., Washenfelder, R. A., Brown, S. S., and Osthoff, H. D.: A broadband cavity-enhanced spectrometer for atmospheric trace gas measurements and Rayleigh scattering cross sections in the cyan region (470-540 nm), *Atmospheric Measurement Techniques*, 12, 1277-1293, 10.5194/amt-12-1277-2019, 2019.
- Kalberer, M., Ammann, M., Arens, F., Gäggeler, H. W., and Baltensperger, U.: Heterogeneous formation of nitrous acid (HONO) on soot aerosol particles, *J. Geophys. Res.-Atmos.*, 104, 13825-13832, 10.1029/1999jd900141, 1999.

- Kleffmann, J., Lorzer, J. C., Wiesen, P., Kern, C., Trick, S., Volkamer, R., Rodenas, M., and Wirtz, K.: Intercomparison of the DOAS and LOPAP techniques for the detection of nitrous acid (HONO), *Atmos. Environ.*, **40**, 3640-3652, 10.1016/j.atmosenv.2006.03.027, 2006.
- Legrand, M., Preunkert, S., Frey, M., Bartels-Rausch, T., Kukui, A., King, M. D., Savarino, J., Kerbrat, M., and Jourdain, B.: Large mixing ratios of atmospheric nitrous acid (HONO) at Concordia (East Antarctic Plateau) in summer: a strong source from surface snow?, *Atmos. Chem. Phys.*, **14**, 9963-9976, 10.5194/acp-14-9963-2014, 2014.
- Longfellow, C. A., Ravishankara, A. R., and Hanson, D. R.: Reactive uptake on hydrocarbon soot: Focus on NO<sub>2</sub>, *J. Geophys. Res.-Atmos.*, **104**, 13833-13840, 10.1029/1999jd900145, 1999.
- Min, K. E., Washenfelder, R. A., Dubé, W. P., Langford, A. O., Edwards, P. M., Zarzana, K. J., Stutz, J., Lu, K., Rohrer, F., Zhang, Y., and Brown, S. S.: A broadband cavity enhanced absorption spectrometer for aircraft measurements of glyoxal, methylglyoxal, nitrous acid, nitrogen dioxide, and water vapor, *Atmos. Meas. Tech.*, **9**, 423-440, 10.5194/amt-9-423-2016, 2016.
- Nakashima, Y., and Sadanaga, Y.: Validation of in situ Measurements of Atmospheric Nitrous Acid Using Incoherent Broadband Cavity-enhanced Absorption Spectroscopy, *Anal. Sci.*, **33**, 519-524, 10.2116/analsci.33.519, 2017.
- Thaler, R. D., Mielke, L. H., and Osthoff, H. D.: Quantification of Nitryl Chloride at Part Per Trillion Mixing Ratios by Thermal Dissociation Cavity Ring-Down Spectroscopy, *Anal. Chem.*, **83**, 2761-2766, 10.1021/ac200055z, 2011.
- Vandaele, A. C., Hermans, C., Simon, P. C., Carleer, M., Colin, R., Fally, S., Mérienne, M. F., Jenouvrier, A., and Coquart, B.: Measurements of the NO<sub>2</sub> absorption cross-section from 42000 cm<sup>-1</sup> to 10000 cm<sup>-1</sup> (238–1000 nm) at 220 K and 294 K, *J. Quant. Spectrosc. Radiat. Transfer*, **59**, 171-184, 10.1016/S0022-4073(97)00168-4, 1998.
- Werle, P., Mucke, R., and Slemr, F.: The Limits of Signal Averaging in Atmospheric Trace-Gas Monitoring by Tunable Diode-Laser Absorption-Spectroscopy (TDLAS), *Applied Physics B-Photophysics and Laser Chemistry*, **57**, 131-139, 10.1007/BF00425997, 1993.
- Wild, R. J., Edwards, P. M., Dube, W. P., Baumann, K., Edgerton, E. S., Quinn, P. K., Roberts, J. M., Rollins, A. W., Veres, P. R., Warneke, C., Williams, E. J., Yuan, B., and Brown, S. S.: A Measurement of Total Reactive Nitrogen, NO<sub>x</sub>, together with NO<sub>2</sub>, NO, and O<sub>3</sub> via Cavity Ring-down Spectroscopy, *Environm. Sci. Technol.*, **48**, 9609-9615, 10.1021/es501896w, 2014.



# Quantification of nitrous acid (HONO) and nitrogen dioxide (NO<sub>2</sub>) in ambient air by broadband cavity-enhanced absorption spectroscopy (IBBCEAS) between 361 – 388 nm

Nick Jordan<sup>1</sup> and Hans D. Osthoff<sup>1</sup>

5 <sup>1</sup> Department of Chemistry, University of Calgary, 2500 University Drive N.W., Calgary, Alberta, Canada T2N 1N4  
*Correspondence to:* Hans D. Osthoff (hosthoff@ucalgary.ca)

## Abstract

This work describes a ~~state-of-the-art~~ incoherent broadband cavity-enhanced absorption spectroscopy (IBBCEAS) instrument for quantification of HONO and NO<sub>2</sub> mixing ratios in ambient air. The instrument  
10 is operated in the near-ultraviolet spectral region between 361 and 388 nm. The mirror reflectivity and optical cavity transmission function were determined from the optical extinction observed when sampling air and helium. To verify the accuracy of this approach, Rayleigh scattering cross-sections of nitrogen and argon were measured and found in quantitative agreement with literature values. The mirror reflectivity exceeded 99.98%, at its maximum near 373 nm, resulting in an absorption pathlength of 6 km -from a 1 m  
15 long optical cavity. The instrument precision was assessed through Allan variance analyses and showed minimum deviations of  $\pm 58$  pptv and  $\pm 210$  pptv ( $1\sigma$ ) for HONO and NO<sub>2</sub>, respectively, at an optimum acquisition time of 5 min. Measurements of HONO and NO<sub>2</sub> mixing ratios in laboratory-generated mixtures by IBBCEAS were compared to thermal dissociation cavity ring-down spectroscopy (TD-CRDS) data and agreed within combined experimental uncertainties. Sample ambient air data collected in Calgary are  
20 presented.

## 1 Introduction

Nitrous acid (HONO) has long been recognized as an important tropospheric oxide of nitrogen (Nash, 1974). Photodissociation of HONO produces the hydroxyl radical (OH); this pathway can be a more  
25 important OH radical source (>10 times greater) than the photolysis of O<sub>3</sub> to O(<sup>1</sup>D) and subsequent reaction with water, especially in polluted urban environments (Harrison et al., 1996; Ren et al., 2006; Alicke et al., 2002). Despite the importance of HONO, accurate and time-resolved (i.e., < 5 min) in situ measurements of ambient HONO mixing ratios remain a challenge, exemplified by discrepancies reported among individual instruments in recent inter-comparison studies (Rodenas et al., 2013; Pinto et al., 2014; Crilley  
30 et al., 2019). These discrepancies arise in part as atmospheric HONO measurements by wet chemical techniques or mass spectrometry require external calibration and are prone to interferences. For instance, long path absorption photometry (LOPAP), while sensitive with limits of detection (LODs) of < 1 parts-per-trillion (10<sup>-12</sup>, pptv), is prone to interference from atmospheric NO<sub>2</sub> and O<sub>3</sub> and (partial) conversion of peroxyacetyl nitrate (PAN) (Villena et al., 2011) and peroxyxynitric acid (HO<sub>2</sub>NO<sub>2</sub>) (Legrand et al., 2014). In  
35 practice, the interference from NO<sub>2</sub> and O<sub>3</sub> can be accounted for with a two-channel system and interference from PAN can be avoided by sampling at low pH (Kleffmann et al., 2006). Interference from HO<sub>2</sub>NO<sub>2</sub> is likely only significant in cold environments such as the poles since this compound is prone to thermal decomposition (Legrand et al., 2014). In contrast, spectroscopic methods that observe HONO directly are less prone to interferences because concentrations are derived from first principles (i.e., the Beer-Lambert  
40 law and known absorption cross-sections) and do not need to rely on external calibration. The prime example is open-path differential optical absorption spectroscopy (DOAS), with LODs typically in the range of 10 – 100 pptv with integration times of several minutes (Tsai et al., 2018). A considerable advantage of open-path instruments is the lack of any inlet and associated chemistry, such as loss of HONO due to partitioning onto inlet walls (Duan et al., 2018) or HONO formation, for example from reaction of  
45 NO<sub>2</sub> with soot particles (Longfellow et al., 1999; Kalberer et al., 1999; Indarto, 2012) that may have deposited on the inlet lines and particle filter. Open-path DOAS, however, only provides concentrations averaged over ~~the a~~ multiple km long absorption path. Spectroscopic techniques that have been used for HONO quantification in situ include Fourier transform infrared (FTIR) spectroscopy (Hanst et al., 1982), tuneable diode laser spectroscopy (TDLS) (Schiller et al., 2001), cavity ring-down spectroscopy (CRDS)  
50 (Wang and Zhang, 2000), and infrared quantum cascade laser (QCL) absorption spectroscopy (Lee et al., 2011). With the exception of the QCL instrument, LODs of these techniques are in the parts-per-billion (10<sup>-9</sup>, ppbv) range which is insufficient to quantify HONO at many locations. Improved LODs are desirable for quantification of HONO in less polluted environments, in particular during daytime, when few techniques are sufficiently sensitive and responsive to study the highly variable and often low mixing ratios.

55 In recent years, the incoherent broadband cavity-enhanced absorption spectroscopy (IBBCEAS) technique  
has been applied to the quantification of HONO and demonstrated improved LODs (e.g., 600 pptv in 20 s  
by Donaldson et al. (2014); 760 pptv in 10 s by Scharko et al. (2014); 175 pptv in 5 s by Min et al. (2016);  
and 90 pptv in 30 s by Duan et al. (2018); Table 1). The IBBCEAS technique operates on the principle that  
the absorption pathlength is enhanced by an optical cavity usually constructed from two reflective mirrors  
60 (Fiedler et al., 2003). Typically, effective absorption pathlengths of a few to several tens of kilometres can  
be obtained from a 0.5–2 m long optical cavity. A large source of uncertainty in the retrieval of mixing  
ratios is knowledge of relevant absorption cross-sections and their convolution to each spectrometer's  
resolution. Other sources of systematic error in IBBCEAS instruments include the determination of the  
mirror reflectivity curve and, if purge gases are used to prevent contact of the sampled gas with the mirrors,  
65 the length over which the absorber is present ( $d_0$ ) compared to the total optical pathlength ( $d$ ) (Duan et al.,  
2018). To exemplify these challenges, a recent inter-comparison study (Crilley et al., 2019) has revealed  
significant biases in the retrieved mixing ratios between two modern IBBCEAS instruments, implying that  
IBBCEAS instruments must be validated.

In this work, we report a new IBBCEAS instrument for quantification of HONO and NO<sub>2</sub> in ambient air,  
70 nicknamed "HONO detection by optical resonance" (HODOR). We present measurements of Rayleigh  
scattering cross-sections of N<sub>2</sub> and Ar in the 350 to 400 nm region. The instrument's precision and optimum  
signal averaging time were assessed through Allan variance analyses (Werle et al., 1993). Using laboratory-  
generated air mixtures, we compared HODOR HONO and NO<sub>2</sub> measurements to a thermal dissociation  
cavity ring-down spectroscopy (TD-CRDS) instrument, which quantified mixing ratios of NO<sub>2</sub> via its  
75 absorption at 405 nm and of HONO via thermal dissociation to NO at 600 °C and subsequent titration of  
NO to NO<sub>2</sub> in excess O<sub>3</sub>. Sample IBBCEAS measurements of ambient air in Calgary are presented.

## 2 Materials and methods

### 2.1 IBBCEAS setup

80 A schematic of HODOR is shown in Fig. 1a. The instrument is comprised of a light source, collimating  
optics, a resonant cavity, an optical filter, a fibre collimator, a specialized fibre bundle, and a grating  
spectrometer. Many instrument components, including the sample cell design, are identical to the  
instrument described by Jordan et al. (2019) with differences noted below.

The light source is an ~~intermediate footprint~~ [emitting area](#) (1.4×1.4 mm<sup>2</sup>), high optical output power  
85 (1150 mW minimum; 1400 mW typical), light emitting diode (LED) (Thorlabs M365LP1, Newton, NJ,  
USA) equipped with a heat sink. A single thermoelectric module (CUI Inc. CP30238, Tualatin, Oregon,

USA) is mounted between the LED and its heat sink such that the module is only ~3 cm away from the LED chip. The LED temperature is controlled by a PID controller (Omega CNI3253) and stabilized to 25.00±0.05 °C with the aid of a K-type thermocouple (Omega) situated ~0.5 cm behind the LED chip. At this temperature, the LED output spectrum has a peak wavelength at 367.8 nm and a FWHM of 10.1 nm (Fig. S1).

The LED is coupled to the cavity by a single f/0.89 aspheric condenser lens (Thorlabs ACL2520U-A) with a high numeric aperture (NA = 0.60) to maximize coupling efficiency of the large angular displacement of the LED output rays. In this work, the LED was operated at 68% (1150 mA) of its maximum forward current (~1700 mA). This allows for sufficient light to couple into the cavity such that the integrated IBBCEAS signal (~50000 counts near the peak wavelength) is ~30% below saturation (~70000 counts) for a cavity filled with cylinder "zero" air (80.5% N<sub>2</sub> and 19.5% O<sub>2</sub>, Praxair) at ambient pressure (893.3 hPa).

The optical cavity is constructed from two highly reflective, dielectric mirrors (Advanced Thin Films, Boulder, CO, USA), 2.54 cm in diameter, 0.635 cm thickness, with 1 m radius of curvature, and maximum reflectivity between 360 and 390 nm. The cavity output is collected by an f/3.1 lens (Thorlabs LA4725) and filtered through a coloured glass UV filter (Thorlabs FGUV5M) to remove light outside the range of the highly reflective mirrors. The signal is then imaged onto a 0.5 cm diameter f/2 lens (74-UV; Ocean Optics, Dunedin, FL, USA) that couples light into the round end of a 2 m long, 0.22 NA, 7×200 μm fibre bundle (Thorlabs BFL200HS02). The line end of the fibre bundle is aligned with the entrance slit of a grating imaging spectrograph to optimize coupling and maximize illumination of the spectrometer detector.

The grating spectrometer (spectrograph and camera; [Princeton Instruments Acton SP2156](#)) has been described by Jordan et al. (2019). The spectrograph is configured with a 1200 groove  $\text{mm}^{-1}$  grating, blazed at 500 nm and positioned at 350 nm central wavelength with a spectral coverage from 291.9 to 408.2 nm. The spectrograph is controlled by custom software written in LABVIEW™ (National Instruments). The spectrograph entrance slit width was set at ~100 μm resulting in a ~1 nm spectral resolution, estimated from the emission lines of a Ne lamp directed through the slit. The spectral resolution varied slightly with wavelength: emission lines at 352.05, 359.35, and 375.42 nm exhibited full-widths-at-half-maximum (FWHM) of 1.08±0.02, 0.99±0.01, and 1.02±0.04, respectively (Fig. S2 and Table S1).

The instrument's inlet was constructed from 1/4" (0.635 cm) outer diameter (o.d.) and 3/16" (0.476 cm) inner diameter (i.d.) fluorinated ethylene propylene (FEP) Teflon™ tubing (Saint Gobain Plastics), perfluoroalkoxy alkanes (PFA) Teflon™ compression fittings (Entegris Fluid Handling), a 2 μm pore size, 47 mm diameter Teflon™ filter (Pall) housed in a PFA Teflon™ filter holder (Cole Parmer).



## 2.2 Determination of mirror reflectivity

120 We used the method by Washenfelder et al. (2008) to determine  $R(\lambda)$ . Briefly, the method requires measuring the optical extinction of two high purity gases with known scattering cross-sections. The mirror reflectivity is then calculated from

$$R(\lambda) = 1 - d \frac{\alpha_{Ray}^{air}(\lambda) \frac{I_{air}(\lambda)}{I_{He}(\lambda)} - \alpha_{Ray}^{He}(\lambda)}{1 - \frac{I_{air}(\lambda)}{I_{He}(\lambda)}} . \quad (1)$$

Here,  $R(\lambda)$  is the wavelength dependent mirror reflectivity,  $\alpha_{Ray}^X(\lambda)$ , is the extinction coefficient due to Rayleigh scattering,  $I_X(\lambda)$  is the measured signal intensity in the presence of non-absorbing, scattering gas molecules, and  $d$  is the cavity length.

For ambient air measurements in this work, we filled the optical cavity using air ("zero" grade, 19.5% O<sub>2</sub> and 80.5% N<sub>2</sub>, Praxair) and with He (Praxair, 99.999%) via the purge ports and used the scattering cross-sections of air from Bodhaine et al. (1999) and those of Cuthbertson and Cuthbertson (1932) for He. For the measurement of the Ar scattering cross-sections, the mirror reflectivity was obtained from the dispersion of N<sub>2</sub> and He, the literature scattering cross-sections of N<sub>2</sub> (Peck and Khanna, 1966) and He (Cuthbertson and Cuthbertson, 1932). The scattering cross-sections of N<sub>2</sub> were determined from the mirror reflectivity based on the dispersion by Ar (Peck and Fisher, 1964) and He.

## 2.3 Operation of HODOR

135 The instrument was turned on 30 min prior to measurements to allow for the LED temperature to stabilize and the CCD camera to cool to its operating temperature of -80 °C. Dark spectra were acquired daily with identical integration time as that of the sample spectra and then averaged to 60 s to represent the dark spectrum applied in the analysis. The dark spectrum was subtracted from raw data spectra as a first step in the data reduction. Air was sampled at a flow rate of 2–3 slpm resulting in a residence time of 5.5–3.6 s.

140 Spectral data were recorded at 1 s integration time and averaged to 10 s. Following data reduction, retrieved mixing ratios were averaged to either 1 or 5 min. He and zero air were sampled for 5 min each day and used to determine the mirror reflectivity (Sec. 3.2). For ambient air measurements, zero air was generated using a custom-built generator (Jordan et al., 2019). The IBBCEAS sampled zero air every 10 min for a duration of 2 min.

## 145 2.4 Reference spectra and spectral fitting

Absorption spectra were calculated as described by Washenfelder et al. (2008) using:

$$\alpha_{abs}(\lambda) = R_L \left( \frac{1-R(\lambda)}{d} + \alpha_{Ray}(\lambda) \right) \left( \frac{I_0(\lambda)-I(\lambda)}{I(\lambda)} \right) \quad (2)$$

Here,  $R_L$  is the ratio of the ~~cell-cavity~~ length ( $d \approx 101$  cm) divided by the length occupied by the sample ( $d_0 \approx 82$  cm - section 3.3),  $\alpha_{Ray}(\lambda)$  is the total extinction due to scattering,  $I_0(\lambda)$  is the intensity spectrum in the absence of absorbers in the cavity cell, and  $I(\lambda)$  is the intensity spectrum measured in the presence of  
 150 absorbers. Zero spectra were interpolated between successive zero determinations by a macro written in Igor Pro software (Wavemetrics, Inc.); this macro also calculated the absorption spectra,  $\alpha_{abs}(\lambda)$ .

Following Tsai et al. (2018), we chose the absorption cross-sections of Stutz et al. (2000) and Vandaele et al. (1998) for HONO and NO<sub>2</sub> retrievals, respectively. These cross-sections were convolved with a sharp  
 155 line at 359.35 nm (observed FWHM = 1.04±0.01 nm) from the emission of a Ne lamp to match the resolution of HODOR (Fig. S2 and Sec. 2.1). The convoluted cross-sections are shown in Fig. S3. Convolution was found to be critical for accurate retrieval of gas-phase concentrations. If omitted, retrieved mixing ratios showed significant (>50%) systematic errors (data not shown).

The retrieval of gas-phase concentrations from the observed absorption spectra was performed with DOAS  
 160 intelligent system (DOASIS) software (Kraus, 2003). ~~Gas concentrations were extracted from a linear least square fit applied to the calculated absorption coefficient, followed by conversion to mixing ratios using the number density of air calculated from the ideal gas law and the temperature and pressure of the sampled gas, monitored using a K-type thermocouple (Omega) and a pressure transducer (MKS Baratron 722B).~~  
 Data were fitted using the convoluted absorption spectra of NO<sub>2</sub> and HONO (Fig. S3) and a third-~~degree~~  
 165 ~~order~~ polynomial from 361 to 388 nm. The spectral shifting setting in DOASIS was set to ±0.1 nm. Stretching was allowed within a margin of ±3%. Since the zero air generator produces scrubbed air at the same relative humidity as in ambient air, absorption by water in this region (Lampel et al., 2017) was negligible in  $\alpha_{abs}(\lambda)$  calculated from Eq. (2). ~~Gas concentrations were extracted from a linear least square fit applied to the calculated absorption coefficient, followed by conversion to mixing ratios using the number density of air calculated from the ideal gas law and the temperature and pressure of the sampled gas, monitored using a K-type thermocouple (Omega) attached to the sample cell holder and a pressure transducer (MKS Baratron 722B) located next to where gases exit the sample cell and upstream of the mass flow controller.~~

## 2.5 Measurement of Rayleigh scattering cross-sections

175 To measure scattering cross-sections, gases were introduced into the IBBCEAS instrument through the purge ports, and the instrument inlet was open to ambient air (while the sample cell exhaust was sealed) to allow other gases to be displaced. The extinction spectrum of each gas was recorded at ambient pressure

and temperature for 10 min at an acquisition rate of 10 s with a 1 s integration of the output intensity signal. The scattering cross-sections were determined from the relationship given by Thalman et al. (2014):

$$180 \quad \alpha_{Ray}^A(\lambda) = \left( \frac{1-R(\lambda)}{a} \right) \left( 1 - \frac{I_A(\lambda)}{I_B(\lambda)} \right) + \alpha_{Ray}^B(\lambda) \left( \frac{I_B(\lambda)}{I_A(\lambda)} \right) \quad (3)$$

Here,  $\alpha_{Ray}^A(\lambda)$  is the scattering coefficient of the gas A in question,  $I_A(\lambda)$  and  $I_B(\lambda)$  are the IBBCEAS signal intensities measured individually for two different gases, and  $\alpha_{Ray}^B(\lambda)$  is the scattering coefficient of gas B which is found from a known scattering cross-section and the number density calculated from the ideal gas law.

## 185 2.6 Preparation and delivery of NO<sub>2</sub> and HONO

Figure 1c shows the experimental setup used to generate NO<sub>2</sub>. Briefly, NO<sub>2</sub> was generated by mixing the output of a standard NO cylinder ([Scott-Marrin, 101±1 ppmv in oxygen- and moisture-free nitrogen](#)) with O<sub>3</sub> produced by illuminating a flow of O<sub>2</sub> (99.99%, Praxair) by a 254 nm Hg lamp followed by dilution with zero air to vary the product concentration. [When not in use, the setup remained under O<sub>2</sub> flow to prevent moisture and other impurities from contaminating the tubing.](#)

Gas streams containing HONO were produced by dissolving ~0.1 g of sodium nitrite (NaNO<sub>2</sub>) into 5 mL potassium oxalate / oxalic acid (K<sub>2</sub>C<sub>2</sub>O<sub>4</sub>·H<sub>2</sub>O / H<sub>2</sub>C<sub>2</sub>O<sub>4</sub>) buffer solution (pH = 3.74) placed inside a glass trap as illustrated in Fig. 1b. The trap was operated in active mode with a dilution flow of N<sub>2</sub> (99.998%) directed through the trap bypass and controlled by a 50 μm critical orifice which was regulated by a back pressure of 138 kPa. A thin sheath of aluminum was wrapped around the exterior of the trap to reduce HONO photolysis. The sample stream of HONO in N<sub>2</sub> was further diluted downstream in zero air to vary the concentration of HONO. The glass trap, containing the buffer solution and the dissolved NaNO<sub>2</sub>, was placed under constant flow of N<sub>2</sub> for approximately 2 days prior to sampling to remove as much NO and NO<sub>2</sub> as possible. The trap acted as a source of both HONO and NO<sub>2</sub> and allowed for the simultaneous determination of both, while also allowing to capture the influence on the retrievals of HONO in the presence of another gas of high concentration (i.e., NO<sub>2</sub>).

## 200 2.7 Measurement of NO<sub>2</sub> and NO<sub>2</sub> + HONO by TD-CRDS

Mixing ratios of HONO and NO<sub>2</sub> were measured in parallel by HODOR and a compact TD-CRDS instrument equipped with two 55 cm long optical cavities, henceforth referred to as the general nitrogen oxide measurement (GNOM) (Taha et al., 2013). Mixing ratios of NO<sub>2</sub> were quantified through optical absorption at 405 nm by a continuous wave, blue diode laser (Power Technology IQμ2A105, Little Rock,



AR, USA) at 1 s temporal resolution (Paul and Osthoff, 2010; Odame-Ankrah, 2015). Both GNOM channels were equipped with heated quartz inlets for thermal conversion of NO<sub>x</sub> (odd nitrogen; e.g., peroxyacetyl nitrate (PAN), HONO, or HNO<sub>3</sub>) to NO<sub>2</sub>. The cylindrical quartz inlets were 60 cm long, 0.625 cm o.d. and 0.365 cm i.d., and resistively heated using a 14.5 Ω nickel/chromium (Nichrome) alloy wire coiled several tens of times around each quartz tube covering a length of ~30 cm. Temperature was monitored by a K-type thermocouple embedded within the coating material and in direct contact with the quartz surface at the centre of each heated section of the inlet. These quartz tubes were connected to the remaining inlet assembly via PFA Teflon™ compression fittings (Entegris Fluid Handling).

215 When the quartz portion of the inlet is heated above ~300°C, HONO dissociates to NO and OH radicals (Perez et al., 2007). The inlet of the “hot,” channel was heated to 525 °C to ensure complete dissociation of HONO, and occasionally ramped in 15 °C decrements (10 s interval) to lower temperatures. The other, “cold,” channel was kept at a reference temperature of 225 °C.

Following the TD section but prior to entering the CRDS cell, NO (present in the sampled air and generated by TD of HONO) reacted with excess O<sub>3</sub> to NO<sub>2</sub> (Wild et al., 2014). Ozone was produced through illumination of a ~7 sccm flow of O<sub>2</sub> (99.99%) by a 185 nm Hg pen-ray lamp (Jelight, Irvine, CA, USA). After mixing with the sampled air, the O<sub>3</sub> mixing ratio was ~8 parts-per-million (ppm, 10<sup>-6</sup>), measured off-line by optical absorption using a commercial instrument (Thermo 49i). A box model simulation (not shown) was carried out to verify that (a) NO is fully titrated by the time the sampled air enters the cavity, and (b) that loss of NO<sub>2</sub> to oxidation by O<sub>3</sub> is small. The simulation showed that under the conditions employed here, the conversion efficiency of NO to NO<sub>2</sub> was less than unity, ~83.8% when averaged over the length of the optical cavity, because the sampled gas entered the cavity prior to complete titration of NO to NO<sub>2</sub>. The TD-CRDS HONO data were hence scaled by a factor of 1/0.838 = 1.194 prior to presentation. The accuracy of this correction factor is limited by knowledge of the rate coefficient for the oxidation of NO by O<sub>3</sub>, ±10% (Burkholder et al., 2015).

Figure S4 shows a sample TD-CRDS inlet temperature scan when the output of the source described in Sec. 2.6 was sampled. In this particular example, the heated channel (to which excess O<sub>3</sub> was continuously added) measured ~137.5 ppbv of NO<sub>y</sub> (NO<sub>x</sub> + HONO) while the cold channel measured ~108 ppbv NO<sub>2</sub> originating from the glass trap. When the hot channel temperature was cooled to a temperature of 350 °C, the same amount of NO<sub>2</sub> was observed in both channels.

## 2.8 Sample ambient air measurements

Ambient air was sampled by HODOR at the "Penthouse" laboratory located on the rooftop of the Science B building at the University of Calgary (latitude 51.0794 °N, longitude -114.1297 °W, ~25 m above ground level) on 27-30 April 2018. This site was the location of several earlier studies (Mielke et al., 2011; Odame-Ankrah and Osthoff, 2011; Woodward-Massey et al., 2014; Mielke et al., 2016) and exhibits NO<sub>x</sub> levels in the 10s of ppbv range typical of urban environments. The instrument sampled from a 1.8 m long FEP Teflon™ inlet at a flow rate of 2 slpm, of which ~1/3 was guided through a partially open window.

### 3 Results

#### 3.1 Determination of mirror reflectivity $R(\lambda)$

Figure 2a shows the IBBCEAS signal intensities for a cavity filled with air, N<sub>2</sub> and He, as well as the respective literature scattering cross-sections; Fig. 2b shows  $R(\lambda)$  (~0.99981 near 373 nm) and the absorption path enhancement (~6 km) from the 1.01 m long cavity. Repeated measurements of  $R(\lambda)$  over a 1-week period showed a standard deviation of  $\pm 0.000003$  (at maximum  $R$ ). From this, it was judged that one daily measurement of  $R(\lambda)$  suffices for accurate retrieval of mixing ratios.

The choice of N<sub>2</sub> and He in the determination of  $R(\lambda)$  assumes that their cross-sections are well known but nevertheless may introduce a systematic bias. To validate the above approach, scattering cross-section of N<sub>2</sub> and Ar were measured and examined for their consistency.

#### 3.2 Rayleigh scattering cross-sections of N<sub>2</sub> and Ar in the near-UV

Figure 3 shows the extinction cross-sections of N<sub>2</sub> and Ar, in the 352–398 nm range at a pressure of 881.9±0.7 hPa and temperature of 298.0±0.1 K, along with literature values. The 1 $\sigma$  uncertainty of the IBBCEAS data ( $\pm 2.5\%$ ) was mainly limited by the uncertainty in the measurement of the mirror reflectivity ( $\pm 2.3\%$ ).

Figure 3a shows the IBBCEAS derived scattering cross-sections of N<sub>2</sub>. Superimposed are the refractive index-based (n-based) literature cross-sections of Peck and Khanna (1966) with a King correction factor from Bates (1984) and the nephelometer data of Shardanand and Rao (1977). The observed cross-sections are slightly larger than the n-based values near the extreme wavelengths where the mirror reflectivity is smaller: For example, the IBBCEAS cross-section is larger by +2.0% at 355.03 nm and by +0.02% at 395.08 nm relative to the n-based cross-section. On the other hand, the nephelometer data underestimate both the IBBCEAS and the n-based data at 363.8 nm by 7.4% and 6.5%, respectively, but agree with the other methods within their measurement uncertainty of  $\pm 11\%$  (Table 2).

Figure 3b shows the scattering cross-sections of Ar. Superimposed are the n-based scattering cross-sections calculated from the data of Peck and Fisher (1964) and King correction factor from Bates (1984), as well as the CRDS data of Thalman et al. (2014). Similar to N<sub>2</sub>, the IBBCEAS scattering cross-sections of Ar are marginally smaller than those of the n-based predictions, with larger difference (up to -2.0%) at shorter wavelengths. The nephelometer data at 363.8 nm differ by +4.9% and +5.9% from the IBBCEAS and n-based data but are within their uncertainty of ±11% (Table 2). The IBBCEAS cross-section of Ar at 370.0 nm agrees with the measurement by Thalman et al. (2014), i.e., 2.02×10<sup>-26</sup> cm<sup>2</sup> molecule<sup>-1</sup>.

The scattering cross-sections of N<sub>2</sub>, and Ar measured in this work were consistent with literature values (Table 2). The IBBCEAS measurement verified that both refractive index based and IBBCEAS observed scattering cross-section can be used to calibrate the mirror reflectivity.

### 3.3 Determination of the effective absorption path

The effective absorption path ( $d_0$ ) requires determination in IBBCEAS experiments that use purge volume to maintain mirror cleanliness. The ratio of  $d/d_0$  was determined by sampling oxygen (99.99%, Praxair) and monitoring the absorption of the weakly bound molecular oxygen complex, whose concentration was retrieved using cross-sections by Thalman and Volkamer (2013). When N<sub>2</sub> or zero air was used as a purge gas,  $d_0$  can be calculated directly from this absorption. A slower but (perhaps) more accurate approach is to turn the purge flows off and on. Following Duan et al. (2018),  $d_0$  is then given by:

$$d_0 = d \times \frac{[O_2]_{on}}{[O_2]_{off}} \quad (4)$$

where  $[O_2]_{on}$  and  $[O_2]_{off}$  are the  $[O_2]$  with or without the purge flows. Figure S5 shows  $R_L$  as a function of flow rate. At a flow rate of 2 slpm,  $R_L$  was 1.28±0.05.

### 3.4 Simultaneous retrieval of NO<sub>2</sub> and HONO and comparison of HODOR to TD-CRDS

Figure 4 shows an example fit containing NO<sub>2</sub> and HONO ~~from a sample generated using the HONO generation system described in Sec. 2.6 in ambient air, collected on April 27, 2018, at 01:00 MST~~. The top panel shows the entire absorption (and the fit shown in black) along with the scattering coefficient of air. In this example, NO<sub>2</sub> (shown in blue) and HONO (shown in orange) mixing ratios of ~~109.042.8±0.2~~ ppbv and ~~23.91.9±0.40.2~~ ppbv were obtained, respectively.

Figure 5 shows a time series of NO<sub>2</sub> and HONO mixing ratios (data averaged to 1 min). In this example, the inlet sampled laboratory air or laboratory-generated mixtures of NO<sub>2</sub> and HONO from the glass trap described in Sec. 2.6. The NO<sub>2</sub> mixing ratios observed by IBBCEAS ranged from 0.01 to 124.2 ppbv and

Formatted: Font: 11 pt

295 HONO mixing ratios from 0.01 to 28.2 ppbv. For the time period sampling indoor air, the mixing ratios  
ranged from 16.9 to 48.4 ppbv (median 32.8 ppbv) for NO<sub>2</sub> and from 0.24 to 2.3 ppbv (median 1.1 ppbv)  
for HONO with a median HONO:NO<sub>2</sub> ratio 3.6% these levels are reasonable for an indoor environment  
(Collins et al., 2018). In contrast to the IBBCEAS instrument, the TD-CRDS instrument was unable to  
quantify HONO in indoor air since the high NO<sub>2</sub> background introduces a large subtraction error in the  
300 heated channel. The scatter plot for IBBCEAS vs. CRDS NO<sub>2</sub> data (Fig. S6a) has a slope of  $1.05 \pm 0.01$ , an  
intercept of  $1.5 \pm 0.3$  ppbv and  $r^2$  of 0.990. The scatter plot of IBBCEAS vs. TD-CRDS HONO data (Fig.  
S6b; only data points when the synthetic source was sampled were included in the fit) has a slope of  
 $1.01 \pm 0.01$ , an intercept of  $0.01 \pm 0.24$  ppbv and  $r^2$  of 0.995.

Figure S7 shows a subset of the above data at 1 s time resolution. When switching between sample and zero  
305 periods, the instrument responded rapidly, on the time scale it takes to replace the sampled air from the  
optical cavity, suggesting that the inlets were "well-behaved", i.e., there is no evidence to suggest inlet  
memory effects such as sample loss or production.

### 3.5 Precision, limit of detection and accuracy

Allan deviation analyses (Werle et al., 1993) were carried out to determine the optimum signal averaging  
310 time by continuously sampling zero air through the IBBCEAS cavity, calculating extinction and retrieving  
NO<sub>2</sub> and HONO mixing ratios. This analysis also allows an estimate of the LOD for each molecule [for  
white-noise dominated data \(Werle et al., 1993\)](#). While commonly used amongst IBBCEAS practitioners  
(Thalman and Volkamer, 2010; Langridge et al., 2006; Vaughan et al., 2008; Washenfelder et al., 2008;  
Duan et al., 2018), this approach does not follow the recommended practice by the International Union of  
315 Pure and Applied Chemistry (IUPAC), who recommend repeatedly measuring (at least) one concentration  
near the LOD in addition to the blank (Loock and Wentzell, 2012).

Figure 6 shows the Allan deviation plots with respect to NO<sub>2</sub> and HONO. The Allan deviations after 10, 60  
and 300 s averaging for NO<sub>2</sub> are 1223, 533 and 210 pptv, respectively, with an optimum acquisition time  
(minimum in the Allan deviation plot) of ~15 min. The respective values for HONO are 270, 118 and 58  
320 pptv for the 10, 60 and 300 s acquisition, but with lower optimum acquisition time of ~5 min. Based on the  
above, the LOD ( $2\sigma$ ) for 5 min data was estimated at 420 pptv and 116 pptv for NO<sub>2</sub> and HONO,  
respectively.

Several factors limit the accuracy of IBBCEAS retrievals: the mirror reflectivity ( $\pm 2.3\%$ ),  $R_L$  ( $\pm 5\%$ ), the fit  
retrieval error ( $\pm 2\% - 4\%$ ), the literature absorption cross-sections of HONO ( $\pm 5\%$ ) and NO<sub>2</sub> ( $\pm 4\%$ ),  
325 calibration errors in the sample mass flow controller ( $\pm 1\%$ ), cell pressure ( $\pm 0.7\%$ ) and cell temperature

(±0.5%). Assuming that these errors are independent ~~and random~~, the overall uncertainties, ~~when summed in quadrature~~ (Min et al., 2016), are calculated to 7.3–8.1% and 7.8–8.6% for NO<sub>2</sub> and HONO, respectively.

Not included in this estimate are potential systematic errors resulting from the spectral convolution and fitting procedure (Sect 2.4), ~~and~~ photolysis of the fitted species within the optical cavity, ~~and potential inlet artefacts (which were not characterized under atmospheric conditions)~~. Both NO<sub>2</sub> and HONO can photodissociate when exposed to light in the 360 to 390 nm wavelength region, which is of potential concern in IBBCEAS instruments that utilize ever-more powerful LEDs (Table 1). Calculations of the photolysis frequencies within the optical cavity are challenging because neither the amount of power injected into the optical cavity nor the beam shape (i.e., divergence) are well known. A rough calculation using a mirror reflectivity of  $R(\lambda) \sim 0.9998$  and assuming 500 mW of near-UV light that is coupled into the optical cavity and NO<sub>2</sub> and HONO absorption cross-sections of  $5.5 \times 10^{-19}$  and  $1.2 \times 10^{-19}$  cm<sup>2</sup> molecule<sup>-1</sup>, respectively (Burkholder et al., 2015), gives  $j(\text{NO}_2)$  and  $j(\text{HONO})$  of 0.04 s<sup>-1</sup> and 0.01 s<sup>-1</sup> within the sample region. When the IBBCEAS is operated at a flow rate of 2 slpm, the total residence time is ~5.5 s and sufficiently long that photolysis could occur, biasing the retrieved NO<sub>2</sub> and HONO mixing ratios low. The excellent agreement with CRDS NO<sub>2</sub> and TD-CRDS HONO data and their linear correlation, however, suggest that photodissociation of NO<sub>2</sub> and HONO are negligible. If it had occurred, it could have been suppressed simply by sampling at a ~~faster-higher~~ flow rate.

### 3.8.6 Sample ambient air measurements

Figure 7 shows a time series of ambient air HONO and NO<sub>2</sub> data over a 4-day period, averaged to 5 min. Mixing ratios of NO<sub>2</sub> ranged from 0.6 to 45.1 ppbv (median 6.0 ppbv) and those of HONO from below the detection limit up to 1.97 ppbv (median 0.42 ppbv). Larger HONO mixing ratios were generally observed at night, which is not surprising given the lack of photolysis sinks at that time of day.

A frequently used diagnostic is the HONO:NO<sub>2</sub> ratio (Fig. 7d); its median value was 4.5%, with lower values observed at night (median of 4.0% at 06:00) than during the day (median of 6.2% at 14:00). The nocturnal values are on par with those reported by Wong et al. (2011) for their lowest-elevation light path in Houston, TX, and are thus reasonable. On the other hand, the daytime ratios are surprisingly large. Daytime HONO formation has been an enigma for some time: While traffic emissions generally exhibit HONO:NO<sub>2</sub> ratios of < 2% (Lee et al., 2013), many other daytime sources of HONO have been recognized, including conversion of NO<sub>2</sub> on surfaces containing photosensitizers such as soot (Stemmler et al., 2007) or photolysis of HNO<sub>3</sub> (Zhou et al., 2011), sources that are active near the ground where the IBBCEAS was sampling. The nature of the daytime HONO source is outside the scope of this paper and will be investigated in future studies.

#### 4. Conclusions and future work

360 This paper has described an IBBCEAS instrument for the quantification of HONO and NO<sub>2</sub> in ambient air using their absorption in the 361 – 388 nm wavelength region. The measurement precision ( $2\sigma$ ) was  $\pm 117$  pptv and  $\pm 420$  pptv (300 s) for HONO and NO<sub>2</sub>, respectively, and is on par with recent instruments described in the literature (Table 1). The combination of mirror reflectivity and cavity length produced pathlength of 6 km from a 1 m long cavity, i.e., better than most works with the exception of (Gherman et al., 2008) who used a longer cavity (4.5 m) to achieve a path-length enhancement of 7.5 km and the work of (Scharko et al., 2014) who used slightly more reflective mirrors (99.986% vs. this work's 99.981%) and a cavity of approximately the same length. The 60 s HODOR LOD was 240 pptv and of similar magnitude as the LODs of 180 pptv reported by Duan et al. (2018) and of 200 ~~pppv~~-pptv Nakashima and Sadanaga (2017) and hence on par with state-of-the-art instruments.

370 One of the challenges we encountered in the accurate retrieval of NO<sub>2</sub> and HONO was the convolution procedure and choice of cross-section. Literature values for NO<sub>2</sub> vary by up to  $\pm 6.2\%$  (Harder et al., 1997; Burrows et al., 1998; Vandaele et al., 1998), such that the choice may introduce a systematic bias. In addition, some NO<sub>2</sub> reference spectra have been reported to contain HONO as an impurity (Kleffmann et al., 2006). Though not performed in this work, it may be advisable to use one's own reference spectra in  
375 future IBBCEAS NO<sub>2</sub> and HONO retrievals.

An ongoing issue in the measurement of HONO in ambient air are measurement differences as those described in (Crilley et al., 2019) that are occasionally larger than expected from stated instrumental uncertainties. Mixing ratios measured by the IBBCEAS instrument described in this work were compared with blue diode laser CRDS NO<sub>2</sub> and TD-CRDS HONO and found in agreement. However, the agreement  
380 for HONO was somewhat fortuitous, given that a large TD-CRDS correction factor was necessary to account for undertitration of the NO generated from TD of HONO. Due diligence needs to be exercised in future measurements to verify the accuracy of NO<sub>2</sub> and HONO retrievals.

Though not examined in this work, interferences may arise when sampling for long periods in heavily polluted environments from soot deposition on inlet filters and walls. In such situations, it would be  
385 advisable to monitor inlets for HONO production (or loss) upon aging, for example using a setup as recently described by Duan et al. (2018).

### **Data availability**

The data used in this study are available from the corresponding author upon request  
390 (hosthoff@ucalgary.ca).

### **Author contributions**

NJ and HDO designed the experiments and carried them out.

### **Competing interests**

The authors declare that they have no conflict of interest.

### **395 Acknowledgments**

This work was made possible by the financial support of the Natural Sciences and Engineering Research  
Council of Canada (NSERC) in the form of a Discovery grant (RGPIN/03849-2016), of the Canadian  
Foundation for Innovation (CFI) in the form of a Leadership Opportunity Fund (LOF) grant (#17785), and  
by the Government of Alberta's Advanced Education and Technology (AET) Small Equipment Grants  
400 Program (SEGP; project 10-018-SEG).

## References

- Alicke, B., Platt, U., and Stutz, J.: Impact of nitrous acid photolysis on the total hydroxyl radical budget during the Limitation of Oxidant Production/Pianura Padana Produzione di Ozono study in Milan, *J. Geophys. Res.*, 107, D228196, 10.1029/2000jd000075, 2002.
- 405 Bodhaine, B. A., Wood, N. B., Dutton, E. G., and Slusser, J. R.: On Rayleigh optical depth calculations, *Journal of Atmospheric and Oceanic Technology*, 16, 1854-1861, 10.1175/1520-0426(1999)016<1854:ORODC>2.0.CO;2, 1999.
- Burkholder, J. B., Sander, S. P., Abbatt, J. P. D., Barker, J. R., Huie, R. E., Kolb, C. E., Kurylo, M. J., Orkin, V. L.,  
410 Wilmouth, D. M., and Wine, P. H.: Chemical Kinetics and Photochemical Data for Use in Atmospheric Studies, Evaluation Number 18, National Aeronautics and Space Administration, Jet Propulsion Laboratory, California Institute of Technology, Pasadena, California, 2015.
- Burrows, J. P., Dehn, A., Deters, B., Himmelmann, S., Richter, A., Voigt, S., and Orphal, J.: Atmospheric remote-sensing reference data from GOME: Part I. Temperature-dependent absorption cross-sections of NO<sub>2</sub> in the 231-794  
415 nm range, *J. Quant. Spectrosc. Radiat. Transf.*, 60, 1025-1031, 10.1016/S0022-4073(97)00197-0, 1998.
- Collins, D. B., Hems, R. F., Zhou, S. M., Wang, C., Grignon, E., Alavy, M., Siegel, J. A., and Abbatt, J. P. D.: Evidence for Gas-Surface Equilibrium Control of Indoor Nitrous Acid, *Environm. Sci. Technol.*, 52, 12419-12427, 10.1021/acs.est.8b04512, 2018.
- Crilley, L. R., Kramer, L. J., Ouyang, B., Duan, J., Zhang, W., Tong, S., Ge, M., Tang, K., Qin, M., Xe, P., Shaw, M. D.,  
420 Lewis, A. C., Mehra, A., Bannan, T. J., Worrall, S. D., Priestley, M., Bacak, A., Coe, H., Allan, J., Percival, C. J., Popoola, O. A. M., Jones, R. L., and Bloss, W. J.: Intercomparison of nitrous acid (HONO) measurement techniques in a megacity (Beijing), *Atmos. Meas. Tech. Discuss.*, 10.5194/amt-2019-139, 2019.
- Cuthbertson, C., and Cuthbertson, M.: The refraction and dispersion of neon and helium, *P R Soc Lond a-Conta*, 135, 40-47, 10.1098/rspa.1932.0019, 1932.
- 425 Donaldson, M. A., Berke, A. E., and Raff, J. D.: Uptake of Gas Phase Nitrous Acid onto Boundary Layer Soil Surfaces, *Environmental Science & Technology*, 48, 375-383, 10.1021/es404156a, 2014.
- Duan, J., Qin, M., Ouyang, B., Fang, W., Li, X., Lu, K., Tang, K., Liang, S., Meng, F., Hu, Z., Xie, P., Liu, W., and Häslér, R.: Development of an incoherent broadband cavity-enhanced absorption spectrometer for in situ measurements of HONO and NO<sub>2</sub>, *Atmos. Meas. Tech.*, 11, 4531-4543, 10.5194/amt-11-4531-2018, 2018.
- 430 Fiedler, S. E., Hese, A., and Ruth, A. A.: Incoherent broad-band cavity-enhanced absorption spectroscopy, *Chem. Phys. Lett.*, 371, 284-294, 10.1016/s0009-2614(03)00263-x, 2003.
- Gherman, T., Venables, D. S., Vaughan, S., Orphal, J., and Ruth, A. A.: Incoherent broadband cavity-enhanced absorption spectroscopy in the near-ultraviolet: Application to HONO and NO<sub>2</sub>, *Environm. Sci. Technol.*, 42, 890-895, 10.1021/es0716913, 2008.
- 435 Hanst, P. L., Wong, N. W., and Bragin, J.: A long-path infrared study of Los-Angeles smog, *Atmospheric Environment*, 16, 969-981, 10.1016/0004-6981(82)90183-4, 1982.
- Harder, J. W., Brault, J. W., Johnston, P. V., and Mount, G. H.: Temperature dependent NO<sub>2</sub> cross sections at high spectral resolution, *J. Geophys. Res.-Atmos.*, 102, 3861-3879, 10.1029/96jd03086, 1997.
- Harrison, R. M., Peak, J. D., and Collins, G. M.: Tropospheric cycle of nitrous acid, *Journal of Geophysical Research-Atmospheres*, 101, 14429-14439, 10.1029/96jd00341, 1996.
- 440 Indarto, A.: Heterogeneous reactions of HONO formation from NO<sub>2</sub> and HNO<sub>3</sub>: a review, *Res. Chem. Intermed.*, 38, 1029-1041, 10.1007/s11164-011-0439-z, 2012.



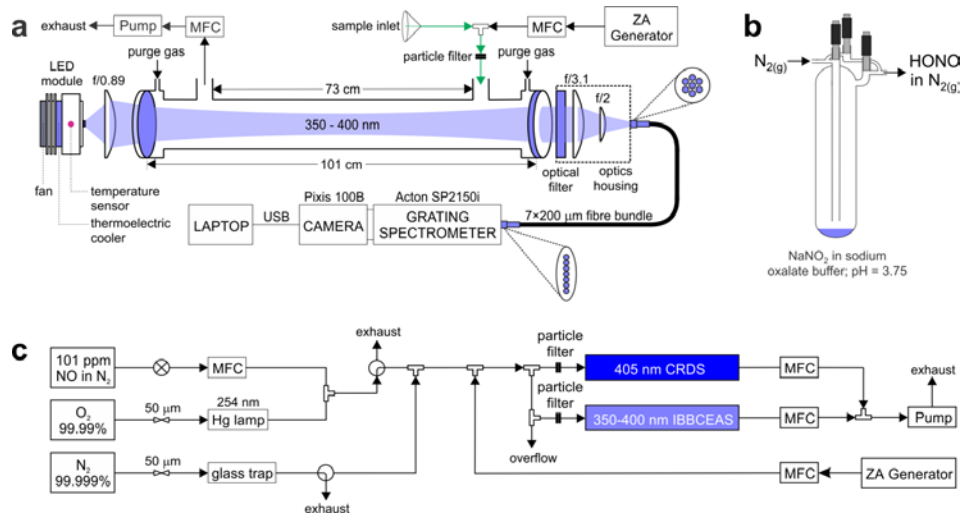
- Jordan, N., Ye, C. Z., Ghosh, S., Washenfelder, R. A., Brown, S. S., and Osthoff, H. D.: A broadband cavity-enhanced spectrometer for atmospheric trace gas measurements and Rayleigh scattering cross sections in the cyan region (470-540 nm), *Atmospheric Measurement Techniques*, 12, 1277-1293, 10.5194/amt-12-1277-2019, 2019.
- 445
- Kalberer, M., Ammann, M., Arens, F., Gäggeler, H. W., and Baltensperger, U.: Heterogeneous formation of nitrous acid (HONO) on soot aerosol particles, *J. Geophys. Res.-Atmos.*, 104, 13825-13832, 10.1029/1999jd900141, 1999.
- Kleffmann, J., Lorzer, J. C., Wiesen, P., Kern, C., Trick, S., Volkamer, R., Rodenas, M., and Wirtz, K.: Intercomparison of the DOAS and LOPAP techniques for the detection of nitrous acid (HONO), *Atmos. Environ.*, 40, 3640-3652, 10.1016/j.atmosenv.2006.03.027, 2006.
- 450
- Kraus, S.: DOAS Intelligent System Version 3.2.3505, Institute of Environmental Physics, University of Heidelberg, available at: <https://doasis.iup.uni-heidelberg.de/bugtracker/projects/doasis/> (last access: 31 August 2018), 2003.
- Lampel, J., Pohler, D., Polyansky, O. L., Kyuberis, A. A., Zobov, N. F., Tennyson, J., Lodi, L., Friess, U., Wang, Y., Beirle, S., Platt, U., and Wagner, T.: Detection of water vapour absorption around 363 nm in measured atmospheric absorption spectra and its effect on DOAS evaluations, *Atmos. Chem. Phys.*, 17, 1271-1295, 10.5194/acp-17-1271-2017, 2017.
- 455
- Langridge, J. M., Ball, S. M., and Jones, R. L.: A compact broadband cavity enhanced absorption spectrometer for detection of atmospheric NO<sub>2</sub> using light emitting diodes, *Analyst*, 131, 916-922, 10.1039/B605636A, 2006.
- Lee, B. H., Wood, E. C., Zahniser, M. S., McManus, J. B., Nelson, D. D., Herndon, S. C., Santoni, G. W., Wofsy, S. C., and Munger, J. W.: Simultaneous measurements of atmospheric HONO and NO<sub>2</sub> via absorption spectroscopy using tunable mid-infrared continuous-wave quantum cascade lasers, *Appl. Phys. B*, 102, 417-423, 10.1007/s00340-010-4266-5, 2011.
- 460
- Lee, B. H., Wood, E. C., Herndon, S. C., Lefer, B. L., Luke, W. T., Brune, W. H., Nelson, D. D., Zahniser, M. S., and Munger, J. W.: Urban measurements of atmospheric nitrous acid: A caveat on the interpretation of the HONO photostationary state, *J. Geophys. Res.*, 118, 12274-12281, 10.1002/2013jd020341, 2013.
- 465
- Legrand, M., Preunkert, S., Frey, M., Bartels-Rausch, T., Kukui, A., King, M. D., Savarino, J., Kerbrat, M., and Jourdain, B.: Large mixing ratios of atmospheric nitrous acid (HONO) at Concordia (East Antarctic Plateau) in summer: a strong source from surface snow?, *Atmos. Chem. Phys.*, 14, 9963-9976, 10.5194/acp-14-9963-2014, 2014.
- 470
- Longfellow, C. A., Ravishankara, A. R., and Hanson, D. R.: Reactive uptake on hydrocarbon soot: Focus on NO<sub>2</sub>, *J. Geophys. Res.-Atmos.*, 104, 13833-13840, 10.1029/1999jd900145, 1999.
- Loock, H. P., and Wentzell, P. D.: Detection limits of chemical sensors: Applications and misapplications, *Sensors and Actuators B-Chemical*, 173, 157-163, 10.1016/j.snb.2012.06.071, 2012.
- 475
- Mielke, L. H., Furgeson, A., and Osthoff, H. D.: Observation of ClNO<sub>2</sub> in a mid-continental urban environment, *Environm. Sci. Technol.*, 45, 8889-8896, 10.1021/es201955u, 2011.
- Mielke, L. H., Furgeson, A., Odame-Ankrah, C. A., and Osthoff, H. D.: Ubiquity of ClNO<sub>2</sub> in the nocturnal boundary layer of Calgary, AB, Canada, *Canadian Journal of Chemistry*, 94, 414-423, 10.1139/cjc-2015-0426, 2016.
- 480
- Min, K. E., Washenfelder, R. A., Dubé, W. P., Langford, A. O., Edwards, P. M., Zarzana, K. J., Stutz, J., Lu, K., Rohrer, F., Zhang, Y., and Brown, S. S.: A broadband cavity enhanced absorption spectrometer for aircraft measurements of glyoxal, methylglyoxal, nitrous acid, nitrogen dioxide, and water vapor, *Atmos. Meas. Tech.*, 9, 423-440, 10.5194/amt-9-423-2016, 2016.

- 485 Nakashima, Y., and Sadanaga, Y.: Validation of in situ Measurements of Atmospheric Nitrous Acid Using Incoherent Broadband Cavity-enhanced Absorption Spectroscopy, *Anal. Sci.*, 33, 519-524, 10.2116/analsci.33.519, 2017.
- Nash, T.: Nitrous acid in the atmosphere and laboratory experiments on its photolysis, *Tellus*, 26, 175-179, 10.3402/tellusa.v26i1-2.9768, 1974.
- 490 Odame-Ankrah, C. A., and Osthoff, H. D.: A compact diode laser cavity ring-down spectrometer for atmospheric measurements of NO<sub>3</sub> and N<sub>2</sub>O<sub>5</sub> with automated zeroing and calibration, *Appl. Spectrosc.*, 65, 1260-1268, 10.1366/11-06384, 2011.
- Odame-Ankrah, C. A.: Improved detection instrument for nitrogen oxide species, Ph.D., Chemistry, University of Calgary, <http://hdl.handle.net/11023/2006>, 10.5072/PRISM/26475, Calgary, 2015.
- 495 Paul, D., and Osthoff, H. D.: Absolute Measurements of Total Peroxy Nitrate Mixing Ratios by Thermal Dissociation Blue Diode Laser Cavity Ring-Down Spectroscopy, *Anal. Chem.*, 82, 6695-6703, 10.1021/ac101441z, 2010.
- Peck, E. R., and Fisher, D. J.: Dispersion of argon, *Journal of the Optical Society of America*, 54, 1362-1364, 10.1364/josa.54.001362, 1964.
- Peck, E. R., and Khanna, B. N.: Dispersion of nitrogen, *Journal of the Optical Society of America*, 56, 1059-1063, 10.1364/josa.56.001059, 1966.
- 500 Perez, I. M., Wooldridge, P. J., and Cohen, R. C.: Laboratory evaluation of a novel thermal dissociation chemiluminescence method for in situ detection of nitrous acid, *Atmos. Environm.*, 41, 3993-4001, 10.1016/j.atmosenv.2007.01.060, 2007.
- 505 Pinto, J. P., Dibb, J., Lee, B. H., Rappengluck, B., Wood, E. C., Levy, M., Zhang, R. Y., Lefer, B., Ren, X. R., Stutz, J., Tsai, C., Ackermann, L., Golovko, J., Herndon, S. C., Oakes, M., Meng, Q. Y., Munger, J. W., Zahniser, M., and Zheng, J.: Intercomparison of field measurements of nitrous acid (HONO) during the SHARP campaign, *Journal of Geophysical Research-Atmospheres*, 119, 5583-5601, 10.1002/2013jd020287, 2014.
- 510 Ren, X. R., Brune, W. H., Mao, J. Q., Mitchell, M. J., Leshner, R. L., Simpas, J. B., Metcalf, A. R., Schwab, J. J., Cai, C. X., Li, Y. Q., Demerjian, K. L., Felton, H. D., Boynton, G., Adams, A., Perry, J., He, Y., Zhou, X. L., and Hou, J.: Behavior of OH and HO<sub>2</sub> in the winter atmosphere in New York city, *Atmospheric Environment*, 40, S252-S263, 10.1016/j.atmosenv.2005.11.073, 2006.
- Rodenas, M., Munoz, A., Alacreu, F., Brauers, T., Dorn, H. P., Kleffmann, J., and Bloss, W.: Assessment of HONO Measurements: The FIONA Campaign at EUPHORE, in: *Disposal of Dangerous Chemicals in Urban Areas and Mega Cities: Role of Oxides and Acids of Nitrogen in Atmospheric Chemistry*, edited by: Barnes, I., and Rudzinski, K. J., NATO Science for Peace and Security Series C-Environmental Security, 45-58, 2013.
- 515 Scharko, N. K., Berke, A. E., and Raff, J. D.: Release of Nitrous Acid and Nitrogen Dioxide from Nitrate Photolysis in Acidic Aqueous Solutions, *Environmental Science & Technology*, 48, 11991-12001, 10.1021/es503088x, 2014.
- Schiller, C. L., Locquiao, S., Johnson, T. J., and Harris, G. W.: Atmospheric measurements of HONO by tunable diode laser absorption spectroscopy, *J. Atmos. Chem.*, 40, 275-293, 10.1023/A:1012264601306, 2001.
- 520 Shardanand, and Rao, A. D. P.: Absolute Rayleigh scattering cross sections of gases and freons of stratospheric interest in the visible and ultraviolet regions, *NASA TN D-8442*, 1977.
- Stemmler, K., Ndour, M., Elshorbany, Y., Kleffmann, J., D'Anna, B., George, C., Bohn, B., and Ammann, M.: Light induced conversion of nitrogen dioxide into nitrous acid on submicron humic acid aerosol, *Atmos. Chem. Phys.*, 7, 4237-4248, 10.5194/acp-7-4237-2007, 2007.

- 525 Stutz, J., Kim, E. S., Platt, U., Bruno, P., Perrino, C., and Febo, A.: UV-visible absorption cross sections of nitrous acid, *J. Geophys. Res.*, 105, 14585-14592, 10.1029/2000JD900003, 2000.
- Taha, Y. M., Odame-Ankrah, C. A., and Osthoff, H. D.: Real-time vapor detection of nitroaromatic explosives by catalytic thermal dissociation blue diode laser cavity ring-down spectroscopy, *Chem. Phys. Lett.*, 582, 15-20, 10.1016/j.cplett.2013.07.040, 2013.
- 530 Thalman, R., and Volkamer, R.: Temperature dependent absorption cross-sections of O<sub>2</sub>-O<sub>2</sub> collision pairs between 340 and 630 nm and at atmospherically relevant pressure, *Phys. Chem. Chem. Phys.*, 15, 15371-15381, 10.1039/c3cp50968k, 2013.
- Thalman, R., Zarzana, K. J., Tolbert, M. A., and Volkamer, R.: Rayleigh scattering cross-section measurements of nitrogen, argon, oxygen and air, *J. Quant. Spectrosc. Radiat. Transfer*, 147, 171-177, 10.1016/j.jqsrt.2014.05.030, 2014.
- 535 Thalman, R. M., and Volkamer, R. M.: Inherent calibration of a blue LED-CE-DOAS instrument to measure iodine oxide, glyoxal, methyl glyoxal, nitrogen dioxide, water vapour and aerosol extinction in open cavity mode, *Atmos. Meas. Tech.*, 3, 1797-1814, 10.5194/amt-3-1797-2010, 2010.
- 540 Tsai, C., Spolaor, M., Colosimo, S. F., Pikelnaya, O., Cheung, R., Williams, E., Gilman, J. B., Lerner, B. M., Zamora, R. J., Warneke, C., Roberts, J. M., Ahmadov, R., de Gouw, J., Bates, T., Quinn, P. K., and Stutz, J.: Nitrous acid formation in a snow-free wintertime polluted rural area, *Atmos. Chem. Phys.*, 18, 1977-1996, 10.5194/acp-18-1977-2018, 2018.
- Vandaele, A. C., Hermans, C., Simon, P. C., Carleer, M., Colin, R., Fally, S., Mérianne, M. F., Jenouvrier, A., and Coquart, B.: Measurements of the NO<sub>2</sub> absorption cross-section from 42000 cm<sup>-1</sup> to 10000 cm<sup>-1</sup> (238–1000 nm) at 220 K and 294 K, *J. Quant. Spectrosc. Radiat. Transfer*, 59, 171-184, 10.1016/S0022-4073(97)00168-4, 1998.
- 545 Vaughan, S., Gherman, T., Ruth, A. A., and Orphal, J.: Incoherent broad-band cavity-enhanced absorption spectroscopy of the marine boundary layer species I<sub>2</sub>, IO and OIO, *Phys. Chem. Chem. Phys.*, 10, 4471-4477, 10.1039/b802618a, 2008.
- Villena, G., Bejan, I., Kurtenbach, R., Wiesen, P., and Kleffmann, J.: Development of a new Long Path Absorption Photometer (LOPAP) instrument for the sensitive detection of NO<sub>2</sub> in the atmosphere, *Atmos. Meas. Tech.*, 4, 1663-1676, 10.5194/amt-4-1663-2011, 2011.
- 550 Wang, L. M., and Zhang, J. S.: Detection of nitrous acid by cavity ring down spectroscopy, *Environm. Sci. Technol.*, 34, 4221-4227, 10.1021/es0011055, 2000.
- Washenfelder, R. A., Langford, A. O., Fuchs, H., and Brown, S. S.: Measurement of glyoxal using an incoherent broadband cavity enhanced absorption spectrometer, *Atmos. Chem. Phys.*, 8, 7779-7793, 10.5194/acp-8-7779-2008, 555 2008.
- Werle, P., Mucke, R., and Slemr, F.: The Limits of Signal Averaging in Atmospheric Trace-Gas Monitoring by Tunable Diode-Laser Absorption-Spectroscopy (TDLAS), *Applied Physics B-Photophysics and Laser Chemistry*, 57, 131-139, 10.1007/BF00425997, 1993.
- 560 Wild, R. J., Edwards, P. M., Dube, W. P., Baumann, K., Edgerton, E. S., Quinn, P. K., Roberts, J. M., Rollins, A. W., Veres, P. R., Warneke, C., Williams, E. J., Yuan, B., and Brown, S. S.: A Measurement of Total Reactive Nitrogen, NO<sub>y</sub>, together with NO<sub>2</sub>, NO, and O<sub>3</sub> via Cavity Ring-down Spectroscopy, *Environm. Sci. Technol.*, 48, 9609-9615, 10.1021/es501896w, 2014.
- 565 Wong, K. W., Oh, H. J., Lefer, B. L., Rappenglück, B., and Stutz, J.: Vertical profiles of nitrous acid in the nocturnal urban atmosphere of Houston, TX, *Atmos. Chem. Phys.*, 11, 3595-3609, 10.5194/acp-11-3595-2011, 2011.

Woodward-Massey, R., Taha, Y. M., Moussa, S. G., and Osthoff, H. D.: Comparison of negative-ion proton-transfer with iodide ion chemical ionization mass spectrometry for quantification of isocyanic acid in ambient air, *Atmos. Environ.*, 98, 693-703, 10.1016/j.atmosenv.2014.09.014, 2014.

570 Zhou, X., Zhang, N., TerAvest, M., Tang, D., Hou, J., Bertman, S., Alaghmand, M., Shepson, P. B., Carroll, M. A., Griffith, S., Dusanter, S., and Stevens, P. S.: Nitric acid photolysis on forest canopy surface as a source for tropospheric nitrous acid, *Nat. Geosci.*, 4, 440-443, 10.1038/ngeo1164, 2011.



575 **Figure 1** Schematics of: **a)** HODOR optical setup and ambient air sampling system. The optical portion of  
the instrument consists of temperature stabilized LED module, collimating and focusing optics, band-pass  
filter, specialized fibre bundle, grating spectrometer, and a charge-coupled device array detector. Sample  
ambient air is pulled through a 2-4 m long sampling inlet using a diaphragm pump. Zero air (ZA) is  
occasionally switched on from a cylinder or produced by a zero air generator; **b)** a glass trap containing  
580 dissolved  $\text{NaNO}_2$  showing HONO production in the gas phase while sampling in active mode; and **c)**  
laboratory air sampling system for delivery of  $\text{NO}_2$  and HONO for quantification by IBBCEAS and CRDS  
in parallel. -MFC = mass flow controller. USB = Universal serial bus.

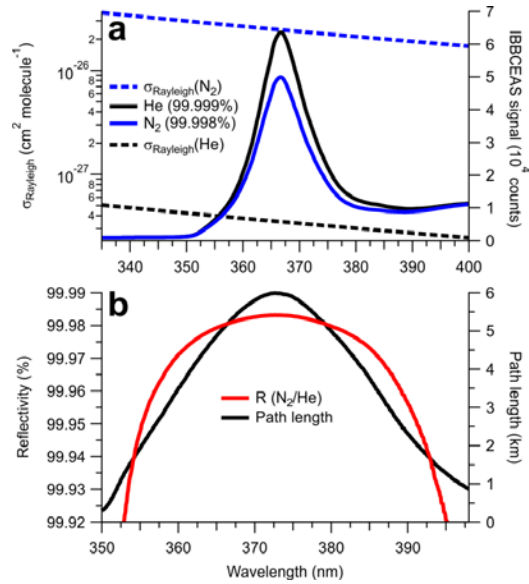
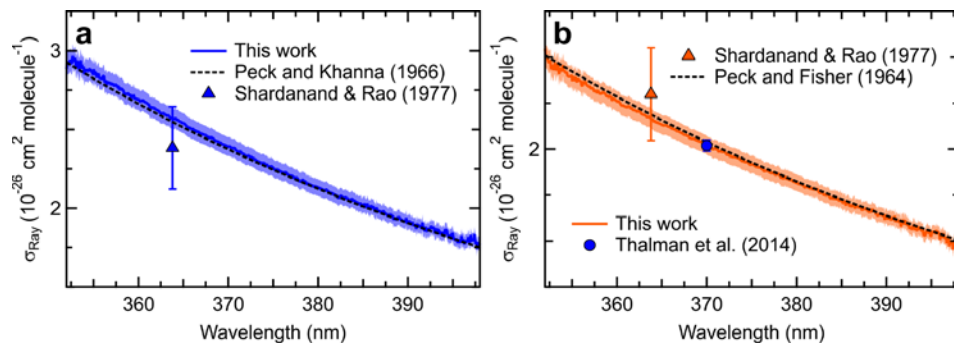
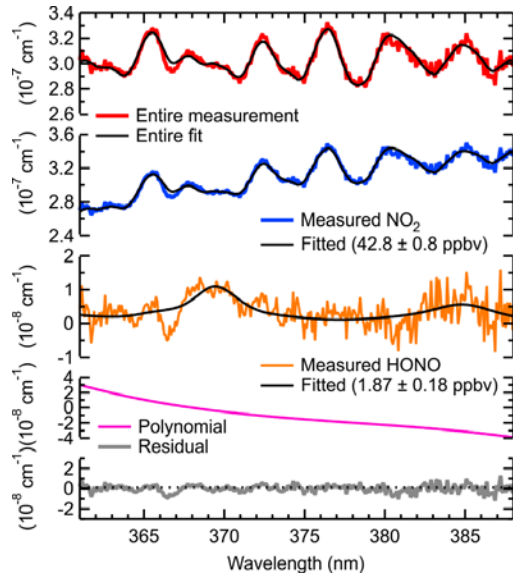


**Figure 2 a)** Cavity output signal for samples of N<sub>2</sub> (99.998%) and He (99.999%), and their scattering cross-sections by Peck and Khanna (1966), and Cuthbertson and Cuthbertson (1932), respectively. The broadband (330–400 nm) cavity output signal is a function of the LED spectral output and the superimposed mirror reflectivity and filter functions. **b)** Reflectivity curve calculated from the ratio of He to N<sub>2</sub> (shown above) using Eq. (2). The effective pathlength,  $d/(1-R)$ , is shown in black.

585

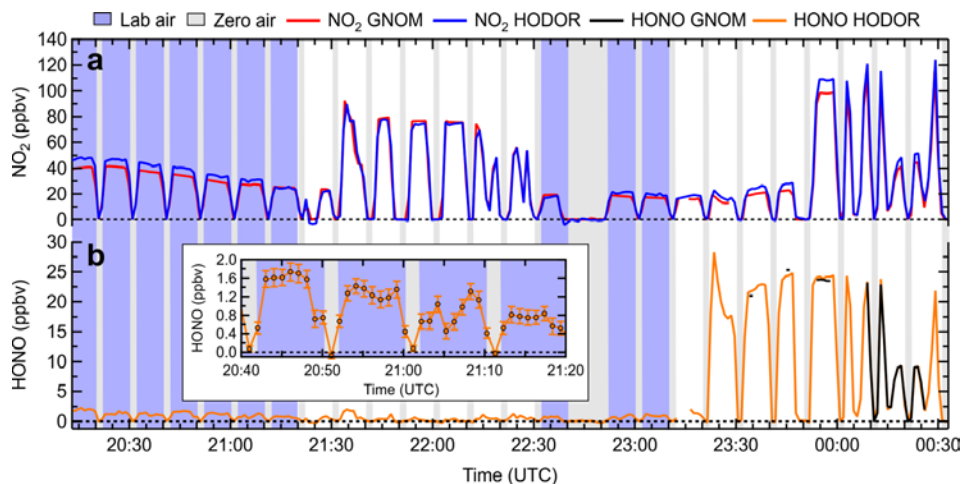


590 **Figure 3** Cross-sections of pure gases: **a)** N<sub>2</sub> (99.998%, in blue), and **b)** Ar (99.998%, orange).



595 **Figure 4** Sample fit for laboratory-generated ambient air containing NO<sub>2</sub> and HONO samples sampled by HODOR at 879.9 hPa and 296 K on April 27, 2018, at 01:00 MST. The top panel shows the entire absorption spectrum. Shown below are the absorption spectra of NO<sub>2</sub> and HONO with their respective fit errors and the polynomial. The bottom panel shows the fit residual.





600 **Figure 5** Time series of NO<sub>2</sub> and HONO mixing ratios observed by HODOR, CRDS and TD-CRDS,  
averaged to 1 min. The instruments sampled for zero air (grey underlay), synthetic and laboratory air (blue  
underlay) and laboratory air to which varying amounts of synthetic air containing NO<sub>2</sub>, HONO and zero air  
were added (white underlay), averaged to 1 min. a) NO<sub>2</sub> mixing ratios reported by IBBCEAS (HODOR,  
blue) and CRDS (GNOM, red). b) HONO mixing ratios reported by TD-CRDS (black) and IBBCEAS  
605 (orange). From 23:30 to 00:10, the TD-CRDS inlet converter temperature was ramped up and down several  
times to collect thermogram; only data collected at an inlet temperature >520 °C are shown here. The inset  
shows the mixing ratio of HONO in laboratory air containing 40–50 ppbv of NO<sub>2</sub>. The error bars show the  
~~±1σ~~ measurement uncertainty of HODOR.

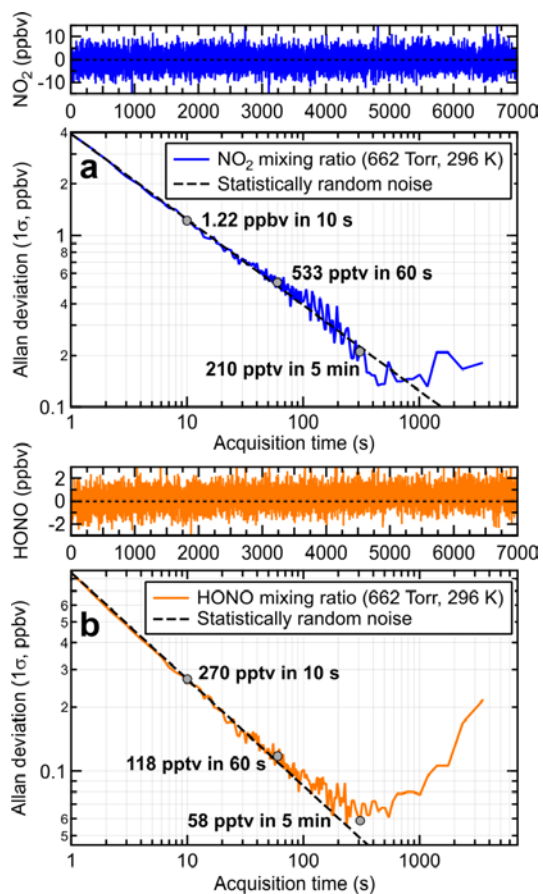


**Figure 6** Allan deviation plots for: **a)** NO<sub>2</sub> and **b)** HONO. The optimum signal averaging time is the inflection point in each variance trace. Each trace was generated by sampling zero air through HODOR for 2 hours at a flow rate of 2 slpm and at ambient pressure (~880 hPa) and temperature (296 K), followed by calculation of the absorption coefficient and fitting the respective convolved absorption cross-sections.

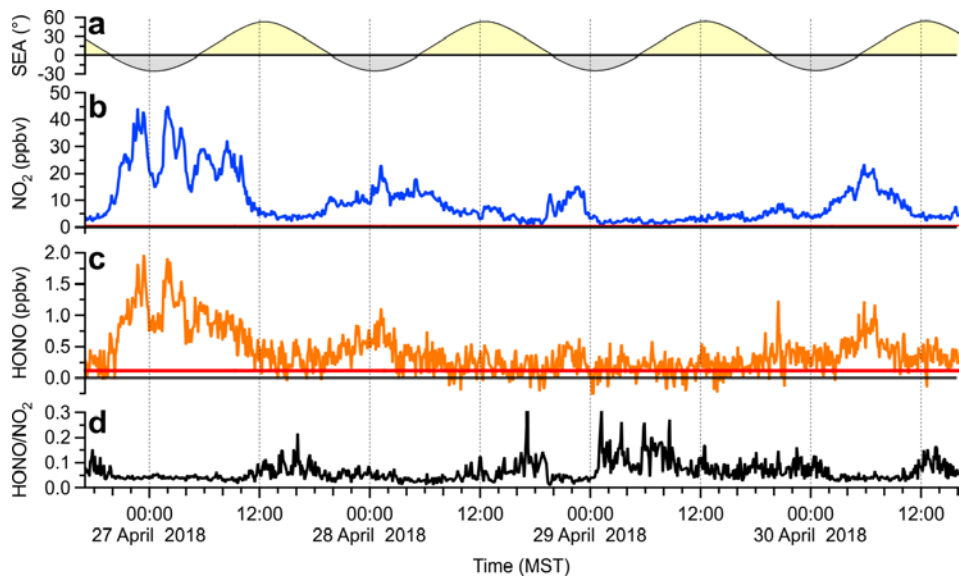


**Figure 7** Time-series of sample ambient air data averaged to 5 min. **a)** Solar elevation angle (SEA) with the yellow and grey shading symbolizing night and day. **b)** IBBCEAS NO<sub>2</sub> mixing ratios **c)** IBBCEAS HONO mixing ratios. The red solid lines indicate the IBBCEAS LOD (2σ level). **d)** HONO:NO<sub>2</sub> ratio calculated from the above. Points below the LOD of HONO were removed from panel d prior to presentation.

**Table 1.** State-of-the-art IBBCEAS instruments for quantification of NO<sub>2</sub> and HONO in the near-UV region.

	365 nm (Gherman et al., 2008)	365 nm (Wu et al., 2014)	368 nm (Donaldson et al., 2014)	368 nm (Scharko et al., 2014)	368 nm (Min et al., 2016)	365 nm (Nakashima and Sadanaga, 2017)	365 nm (Duan et al., 2018)	367 nm (This work)
Light source manufacturer	Omicron Latronics	Nichia Corporation	Nichia Corporation	Nichia Corporation	Nichia Corporation	Thorlabs	LEDengin	Thorlabs
model	n/a	NCSU03AT	n/a	n/a	NCSU033B	M365D1	LZ1-00UV00	M365LP1
optical power (W)	0.105	0.250	0.350	0.350	0.450	0.190	1.68	1.15
$\lambda_p \pm \text{FWHM}^a$ (nm)	365 $\pm$ 12	365 $\pm$ 10	n/a	n/a	368 $\pm$ 8	365 $\pm$ 7.5	365 $\pm$ 13	367 $\pm$ 10
Fit range(s) (nm)	366 – 378	353 – 376	360 – 380	360 – 376	361 – 389	360 – 375	359 – 387	361 – 388
Mirror reflectivity (%)	99.94	99.925	99.976	99.986	99.984	99.985	99.983	99.983
CeH-Cavity length (m)	1.15 or 4.50	1.76	1.022	1.013	0.48	1.0	0.55	1.01
Pathlength <sup>b</sup> (km)	1.9 or 7.5	1.8	4.3	7.2	3.0	4.6	3.2	4.8
Acquisition time (s)	20	120	900	600	60	300	30	60
HONO LOD (2 $\sigma$ , ppbv)	8.0*	1.2	3.0*	1.2*	0.30 <sup>#</sup>	0.2	0.18	0.24*

625 <sup>a</sup> peak wavelength + full-width at half maximum; <sup>b</sup> effective pathlength,  $L_{\text{eff}} = d_0/(1-R)$ ; \* laboratory sample. <sup>#</sup> Field sample

**Table 2.** Summary of observed and literature scattering cross-sections at 363.8 and 370.0 nm.

Gas (Purity)	$\lambda$ (nm)	$\sigma_{Ray}$ (this work) <sup>a</sup> (10 <sup>-26</sup> cm <sup>2</sup> molecule <sup>-1</sup> )	$\sigma_{Ray}$ ( <i>n</i> -based) <sup>b</sup> (10 <sup>-26</sup> cm <sup>2</sup> molecule <sup>-1</sup> )	$\sigma_{Ray}$ (Nephelometer) <sup>c</sup> (10 <sup>-26</sup> cm <sup>2</sup> molecule <sup>-1</sup> )	$\sigma_{Ray}$ (CRDS) <sup>d</sup> (10 <sup>-26</sup> cm <sup>2</sup> molecule <sup>-1</sup> )
N <sub>2</sub> (99.998%)	363.8	2.57	2.55	2.38	-
	370.0	2.39	2.37	-	-
Ar (99.998%)	363.8	2.17	2.19	2.30	-
	370.0	2.02	2.04	-	2.02

<sup>a</sup> The uncertainty is  $\pm 2.5\%$  (see Sec. 3.6); <sup>b</sup> See text for references of *n*-based scattering cross-sections and references therein for corresponding calculations of King correction factors; <sup>c</sup> Data set of (Shardanand and Rao, 1977). <sup>d</sup> Data set

630 of (Thalman et al., 2014); <sup>e</sup> The ratio of N<sub>2</sub>/O<sub>2</sub> in the cylinder was  $\sim 80.5/19.5$ .